16th ICAAR LISBOA 2020-2022
16th International Conference on
Alkali-Aggregate Reaction in Concrete
Lisboa | LNEC | Portugal | 31 May - 2 June 2022
http://icaar2020-2022.lnec.pt

Modelling mechanical effects of AAR and DEF

Alain Sellier (1)

(1) LMDC, INSA/UPS Génie Civil, 135 Avenue de Rangueil, 31077 Toulouse cedex 04 France, alain.sellier@univ-tlse3.fr

Abstract

Resorting to modelling when dealing with the issue of concretes dams, bridges or nuclear power plants affected by AAR (Alkali Aggregate Reaction) or DEF (Delayed Ettringite Formation) is of primary interest, specifically when this is the only way to demonstrate their integrity, and thus have the possibility of keeping them in operation. In this context, the better the realism of the model, the more reliable is the estimation of the residual safety level. Thus, to avoid the environmental impact of a reconstruction and save money, project owners and controllers must invest in increasingly accurate and realistic models. This article provides a non-exhaustive overview of the different ingredients needed to model these problems. The presentation consists from the scale of chemical reactions, to go to the structural level, through homogenization approaches. It concludes with some remarks on the methods of calibration and validation of finite element structural models.

***Keywords**: AAR, calibration, DEF, finite elements, homogenization, modelling, validation.*

1. INTRODUCTION

The ICAAR 10 chairmen have had the kindness to ask me giving a keynote lecture about modelling applied to alkali aggregate reactions (AAR) and delayed ettringite formation (DEF), from a general point of view. I accepted this invitation with pleasure but realise now that this task is more difficult than expected. So, my paper and lecture will not be as extensive as it should be, because it's difficult to stay to be aware of the multiple interesting works over the world on this topic, so be indulgent and please apologize me if your last work are not (yet) cited in this paper! An overview of the last thirty years of the literature on the subject shows that many problems have been treated differently by several research teams all over the world, the reason of this high interest for this very specific topic is that AAR and DEF are phenomena encountered in quasi all countries, and the consequences are always important, specifically because large civil engineering structures like dams, bridges and nuclear power plants are affected, and their replacements are so expensive that any method to repair them and maintain their operability is of great interest. The consequence has been a funding of researches in this domain by many companies of hydroelectricity, highway exploitations, or materials supply. Important engineering companies have also contributed to the development of models able to compute these structures using the finite elements method. Rapidly, engineers dealing with this topic have improved their model, passing in a few years from a thermo-elastic analogy with an isotropic imposed swelling to elastoplastic models with imposed anisotropic swelling depending on stress levels, the empirical law proposed by Charlwood in 1992 [1], which modifies axial swelling versus applied stress, is a good illustration of the rapid progresses done at this time. To validate their models, engineers have collaborated with research laboratories, asking them to build mock-ups with reactive concretes instrumented and stored in controlled conditions of humidity and temperature. The objective was to identify as accurately as possible each influencing parameter on swelling kinetic and amplitude. As often in laboratory, researchers discovered several particularities of AAR: a strong dependence to the applied stresses, an anisotropy of swellings depending not only on axial stress as suggested by Charlwood, but also on the triaxiality rate of the applied loading [2][3][4]. Concerning the DEF, stronger swelling and dependences toward moisture and temperature chronology were observed than for the AAR [5]. The calibration of models was also an important problem mainly due to the slow kinetic of these chemical phenomena in the field. To address this last one, laboratories proposed accelerated swelling tests on concretes specimens drilled in the real structures. But, to obtain significant results in a reasonable duration, they used the thermal activation and the chemical activation of the reactions. As thermodynamic equilibriums vary with temperature and chemical environment, accelerated tests change also the composition of AAR gel [6], and the accelerated tests are finally no so representative of swelling in the real structure as expected [7]. For reactive specimens loaded in laboratories (cylinders, cubes, beams…), the creep of concrete presents sometimes compressive deformations

greater then swelling in free conditions [8], so the interaction between creep and swellings becomes a new subject of research; some researchers think that creep of cement paste could absorb a part of aggregate swelling, pointing out the need to have a better understanding of swelling mechanisms at meso-scale (aggregate's scale) [9]. Concerning swelling, it is now admitted that it is the consequence of micro-cracks propagations at meso-scale, leading to a cracking energy greater than in direct tension. This fact leads to define two type of cracking, the one induced by AAR or DEF, distributed and very dissipative in terms of fracture energy, and the structural crack in tension, localized and lower dissipative [10], but with greater consequences in terms of permeability and durability of structures; specifically, for structures in direct contact with liquid water. The partition of the strains into, creep, distributed cracking, and localized cracking, then became a method to develop realistic models [11]–[13][11]. Concerning the model's calibration; the control of AAR gel composition shows a great variety of alkali and calcium contents, leading to different degrees of solidification: some AAR products obtained in laboratories being gels, other being more or less crystallized [14]. The variety of gels observed by microscopy confirms that any change in environmental conditions, compared to in the field ones, leads to a different product more or less able to migrate into the concrete porosity and into the micro-cracks, and leading to perceptible changes in terms of swelling at macro-scale [15]. Other problems such as interactions with reinforcements [11], reductions of mechanical properties [16] (different in tension and in compression), were underlined by laboratories and engineers, and have to be considered in models. Simultaneously, computing power of computers increase with the progresses of parallel computing, allowing a new class of numerical models with more and more physical meanings. Finally, AAR and DEF are interesting phenomena not only because they concern important civil engineering structures, but also because they offer to researchers an interesting case of study to improve modelling usable in several branch of mechanics, specifically in the domain of coupling between chemical, physical, and mechanical models. From this point of view, AAR and DEF are both a real engineering challenge but also motivating and interesting case studies for academic research dealing with multi-physics modelling methods, with much wider advantages than their applications to AAR or DEF. So, the resulting models are not only interesting tools for engineers, they are also tools to capitalize research's results, and the conferences like ICAAR the way to disseminate them.

These multiple motivations to perform researches on numerical modelling of effects of AAR and DEF are certainly the key of their worldwide appropriation in academic laboratories. This paper will focus on some aspects of these researches; with the goal to supply a better understanding of current's models' capabilities to non-specialist of numerical methods. After a brief recall of engineering issues, the plan adopted for this paper consists going from nano-scale (chemistry model scale) to meso-scale (aggregates) to finish by models usable at structural scales.

2. CONTEXT

"Living with the expansion" is the title of the "state of the art" presented by Robin Charlwood and Ian Sims in [17]. Their section in [17] follows another one called "*Controlling the reaction"*, in which the authors conclude that despite the limited success to control the alkali aggregate reactions (AAR) in pavements (by drying or Lithium salts), controlling the chemical advancement stays quasi impossible at the core of large concrete structures due to the time needed for acting on moisture or on chemical species concentrations (several centuries would be needed to dry concrete at the core of a dam for example). The main problem is then to manage the structural effects of internal swelling reaction (ISR) in order to plan structural maintenance interventions. For this purpose, in complement of in situ measures, finite element modelling is needed. Among the 37 large dams affected by swelling reactions referenced by the ICOLD [18], 31 are effectively modelled by finite element methods to manage interventions or simply to understand and forecast their behaviour. For dams, the effects of expansions are numerous (upstream movements, excessive leakages, stability, structural cracks, loss of gate's clearance for spillways, and ovalization of unit's generators in power house…). To assess effectiveness of management strategies facing these problems, numerical modelling can be of a great help. The typical problems addressed are, for instance, the effectiveness of slot's cutting, of coating membranes, or of gate's and equipment's adjustments, and of course the assessment of structural integrity wich is a major of concern when dealing with dams, nuclear power plants or bridges.

Progresses in understanding of swelling reactions chemistry in one hand, and in modelling of their structural effects in the other hand, are essential to reach a reasonable trust level in finite element analysis. In [17], Goveski and Yildiz give an interesting example of finite element analysis applied to a

large dam affected by alkali silica reaction (ASR). They question the effectiveness of cut slits, and show that if periodic cracks have the advantage of limiting the level of stresses induced by swelling, they have the disadvantage of accelerating swelling and allowing the propagation of new cracks. In their study, the disadvantages are greater than the advantages, which leads to the conclusion that an intervention consisting of the cutting of slots would be deleterious to the dam they are studying. They conclude that only a precise analysis of the effect of cut slits, based on numerical modelling coupled with in situ observations, can justify or avoid intervention. A similar analysis was applied by Olivier Chulliat, Etienne Grimal and Eric Bourdarot to another dam [17], and leads to the opposite conclusion: slit cutting would be beneficial, but must be accompanied by watertight membranes on the upstream face, a drainage curtain to avoid water overpressures in the concrete of the dam, and prestressed anchors to prevent dislocations of concrete blocks during earthquakes. Similar problems exist for bridges, nuclear power plants, and other major civil engineering works.

To be realistic, a finite element modelling has to consider at minima the following physical phenomena:

- The type of internal swelling reactions (ISR) (Alkali Silica / Aggregates Reactions (ASR/AAR) or/and Delayed Ettringite Formation (DEF) in most of cases), linked to the material properties (alkali content, aggregate's mineralogy, cement paste chemistry and transfer's properties)
- The environmental conditions (temperature and moisture past) which control the kinetic and the amplitude of the swelling reactions [19]–[21]
- The swelling anisotropy in presence of compression loadings [1]
- The creep of concrete which is a long term deformation of same order of amplitude than the free swelling induced by AAR [22], and which is able to absorb a part of the swelling effects [9]
- The consequences of swelling on mechanical properties (Young modulus, strength and fracture energy decrease) [23], [24].
- The type of damage induced by swelling (diffuse damage inside the aggregates, diffuse cracks bridging aggregates trough the cement paste, localized cracks at structural level)[11], [12].

As these phenomena take place at different levels, from micro and nanoscales for the chemistry, to meso scale for the interaction between aggregates and cement paste, and finally at macro scale for the localized cracks in structures, several scales of modelling coexist. The smaller scales, mainly used by researchers, are dedicated to the internal swelling reaction comprehension; the larger ones, used by the practitioners, correspond to structures modelling.

Links between these different scales of modelling is theoretically possible using homogenization methods allowing the up-scaling, but the complexity of the underlying phenomena at micro scale needs simplifications in order to obtain macro modelling able to run on finite element codes applicable to large structures. So, during the last decades, the formulation of macro-models became also a research topic. Today modelling progresses go on both at micro and macro scales, with more and more links between these different scales of modelling, capitalizing knowledges from experimental and theoretical chemistry in one hand and from non-linear mechanics in the other. First, we will draw an overview of the advantages and limits of each scale of modelling, next we will have a look to the possible links between these scales, allowed by numerical and analytic upscaling methods.

3. DIFFERENT SCALES OF MODELLING

As explained above, an overview of modelling methods applied to AAR and DEF has to start at nano scale where the chemical reactions take place, then the spatial distribution of reactive sites can be considered at micro scale, inside aggregates for AAR, in the cement paste and at the aggregate-paste interfaces for the DEF. Once these two first scales crossed, the interactions between aggregates and paste can be considered. This is the domain of micro-mechanic-homogenization methods (analytical and numerical, applied to chemistry as well as to mechanics) which allows to link the local swelling of reactive sites at micro scales to the average swelling at the representative volume scale of concrete.

At the structural scale, the structural modelling used is sometimes based on micro-mechanisms considered at lower scales, but often it is only "phenomenological", that is, it is based solely on experiments at the structural scale. The main challenge today is to bridge these different scales of understanding and modelling.

3.1 Micro scale and chemical aspects

3.1.1 Alkali aggregate reactions (AAR)

Although molecular dynamics appears to be a promising tool for understanding some of the properties of C-S-H [25], its use in the context of AAR and DEF remains limited, and chemical models of AAR or DEF are so far more based on experimental observations summarized by classical chemical models, using mass balance equations and, in the case of def, the thermodynamic equilibrium of chemical phenomena. For example, for the AAR the ASR model proposed in 1981 by Dent Glasser and Kataoka [26] is widely accepted (equations (1) and (2), and used in a context of alkali diffusion coupled with a mass conservation equation (3).

$$H_{0.38}Si0_{2.19} + 0.38NaOH \rightarrow Na_{0.38}SiO_{2.19} + 0.38H_2O \quad (1)$$

$$Na_{0.38}SiO_{2.19} + 1.62NaOH \rightarrow 2Na^+ + H_{1.62}SiO_{3.81}^{2-} \quad (2)$$

These two equations are often summarised in a single mass balance equation:

$$H_{0.38}Si0_{2.19} + 2Na^+ + 2OH^- \rightarrow 2Na^+ + H_{1.62}SiO_{3.81}^{2-} \quad (3)$$

Later, some improvements have been proposed by authors; among the different contributions, the silica gel aging process proposed by Zhenguo Shi, Andreas Leemann, Daniel Rentsch and Barbara Lothenbach [6] confirms the possible replacement of alkali by calcium in ASR products, in agreement with the long term reactivity of some concrete despite their relatively limited alkali content, as already mentioned in [25]. As the more or less fluidity of silica gel depends on its calcium content, the fraction of alkali and calcium in ASR product could change the ability of the gel to migrate into the cracks and then the micro-cracking mechanism at the origin of swelling. Of course, as concrete remains a heterogeneous media, different types of gel can coexist in concrete, some of them are fluids while others change to a crystallized form unable to diffuse.

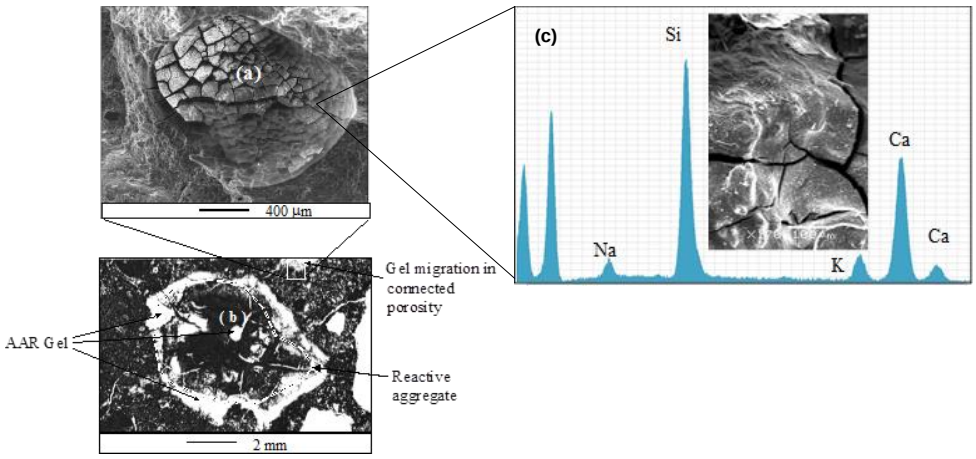

Figure 3.1: (a) AAR gel into the cement paste porosity connected to a reactive aggregate (b), and (c) AAR-gel including calcium observed in a dam's concrete (SEM pictures and EDS analysis from LMDC Toulouse)

As the silica reactivity depends on the basicity of the cement paste, the alkali concentration can be considered as a key variable able to manage the reaction. Another important state variable is the reactive silica content, which, in many structures is so important that, if the $2Na^+ \leftrightarrow Ca^{2+}$ substitution reaction occurs, the swelling could last centuries. Due to the fact that thermodynamic equilibrium of calcium hydrates depend on the temperature [26], the accelerated tests at high temperature have no reason to lead to a same amount of calcium in the AAR gel than in the field at ambient temperature; that is a reason why accelerated tests are so discussed in the literature. This is also the reason why

two types of normalized chemical advancement (A) coexist. Some authors use the alkali consumption [27] (eq.4) while others use the reactive silica consumption (eq.5) [15].

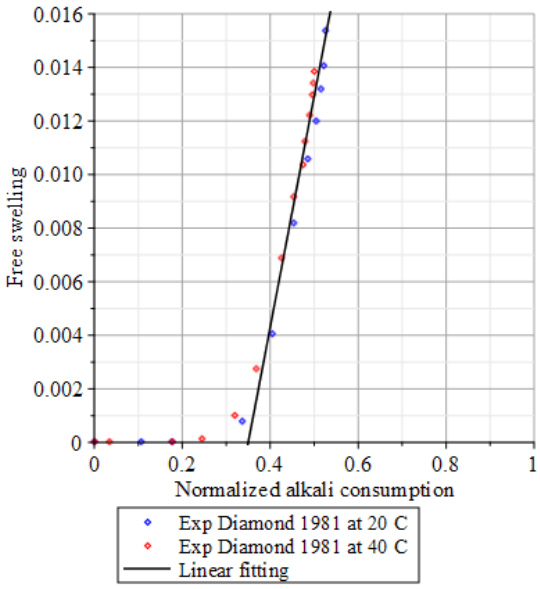

Figure 3.2: Free swelling versus chemical advancement A (defined as the amount of alkaline consumed by the AAR), based on Diamond et al. experimental results [27] as interpreted in ref [28]. A_0 is the swelling threshold defined by Poyet et al. in [19].

Figure 3.2 show an example of evolution of normalized swelling versus the normalized consumption of alkali (equation 4); the curve show that this description is independent of temperature, and it is worth noting the normalized swelling stops for A<1; it means the limited resources are, in these tests, the reactive aggregates, but, in real structures where the reaction occurs at lower pH, due to the substitution of alkali by calcium, the limited resource for the AAR becomes the reactive silica, and it is then preferable to use the advancement defined by equation (5) as in Grimal et al. [10].

$$A(t) = 1 - \frac{Na^{+}(t)_{unreacted}}{Na^{+}(t=0)} \tag{4}$$

$$A(t) = 1 - \frac{SiO_2(t)_{unreacted}}{SiO_2(t=0)} \tag{5}$$

Whatever the definition of the chemical advancement (4) or (5), one of the simplest forms of advancement evolution law is based on the chemical affinity principle (eq.6). This form was proposed by Coussy et al. [29]. In this chemical model two characteristics times are used, a first one τ_l controls the dissolution process (corresponding to the mass balance in eq. 1), and the second τ_c the gel formation (corresponding to eq. 2). This equation is in accordance with the Larive's experimental law used to describe the kinetic of free swelling specimens at macro-scale [30], which presents also these two characteristic times and defines the advancement of the reaction as a normalized free swelling. Close models were developed later following the same principles, for instance the Saouma et al. [31].

$$A = \left(1 - exp\left(-\frac{t}{\tau_c}\right)\right)\left(1 + exp\left(-\frac{t-\tau_l}{\tau_c}\right)\right)^{-1} \tag{6}$$

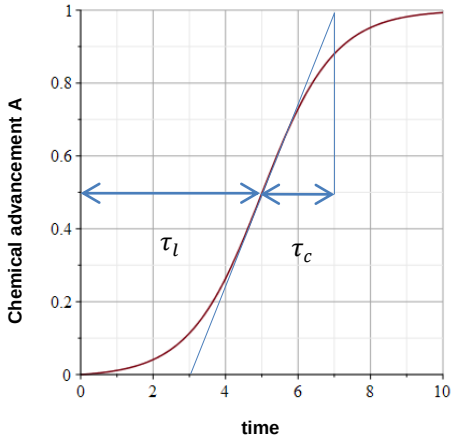

Figure 3.3: General form of the advancement law proposed by C.Larive and O.Coussy [29], [30], (scheme adapted from Saouma et al. chemical model [31])

As the reaction kinetic and amplitude can vary according to the environmental conditions (temperature and humidity) which are themselves variable with time, Poyet et al. [19] proposed using a differential form for the chemical advancement (eq. 7), in which Sr is the water saturation rate, which, according to Poyet et al., limits the reaction amplitude and slows down the kinetic. An illustration of the effect of moisture on AAR is given in Figure 3.10. In [32] Grimal et al. proposed to combine the Arrhenius law fitted on Larive results [30] and the dependence to S_r proposed by S.Poyet et al. to assess the characteristic time τ^c (8); finally in [33] Morenon et al. proposed a last enhancement of this incremental law adding a non-linearity in the moisture influence kinetic term (eq.8 and Figure 3.4). Note Poyet et al. assume that deleterious effects of AAR occur only if the advancement exceeds a chemical threshold noted A_0 corresponding to the volume of gel able to damage the cement paste matrix (Figure 3.4 (a)).

$$\frac{\partial A}{\partial t} = \frac{1}{\tau^c}(Sr - A) \tag{7}$$

$$\tau^c = \tau^c_{ref}\left(\left(\frac{S_r - \bar{S}_r}{1-\bar{S}_r}\right)^2 exp\left(-\frac{Ea}{R}\left(\frac{1}{T}-\frac{1}{T_{ref}}\right)\right)\right)^{-1} \tag{8}$$

In eq.8 $\bar{S}_r \approx 0.1$ is the saturation threshold, $E_a \approx 40kJ/Mol$, the activation energy , $R = 8.31\, J\, Mol^{-1}K^{-1}$. T_{ref} a reference absolute temperature.

Another issue is the effect of pressure on the AAR; in this regard, it is important not to confuse the internal pressure in the porous solution of the concrete with the stress applied by the external load on the concrete volume. According to Hilaire, Giorla, Dunant and Scrivener who performed experimental tests with different imposed interstitial pressures of NaOH solutions (from 0 to 15 MPa) (see [17] pp.56-67), pore pressure does not reduce AAR but, on the contrary, increases the macroscopic swelling of samples immersed in triaxial cells. Thus, the pore pressure of the water is not a limiting factor for AAR (at least up to 15 MPa). This effect of internal pressure should not be confused with the imposed external load which acts by micromechanical processes which modify the microcracking pattern, as explained in point 3.2.2.2, which are capable of reducing swelling without limiting the progress of the chemical reaction.

Current researches about modelling of chemical aspects of AAR concerns the type of product created by the reaction. In accelerated conditions, specifically in laboratories where test are performed with a high alkali content to accelerate silica dissolution, the available calcium is reduced due to the basicity imposed by alkali doping, and the created gel is fluid (exudation of gel at the surface of specimen is then possible), but in situ, where the alkali content is lower, or in laboratories after consumption of

alkali by the first stages of the reaction, the chemical environment of gel is more calcic, leading to the gel transformation to a more crystallized product [6]. The coexistence of these two types of product is not yet managed by simplified modelling such as presented above, but they should be, because the mobility of the AAR gel is a primary factor when dealing with the structural effects of AAR as shown in [12]. In Figure 3.5 a solidified AAR product in a crack is illustrated by a picture provided by S. Feldman (NIST). This observation implies the migration possibility of silica from the aggregate to the crack. These observations show that a global chemical advancement of AAR (such as the state variable A in previous equations) will no more be sufficient to describe the variety of gel, their calcium content linked to their fluidity must be also considered.

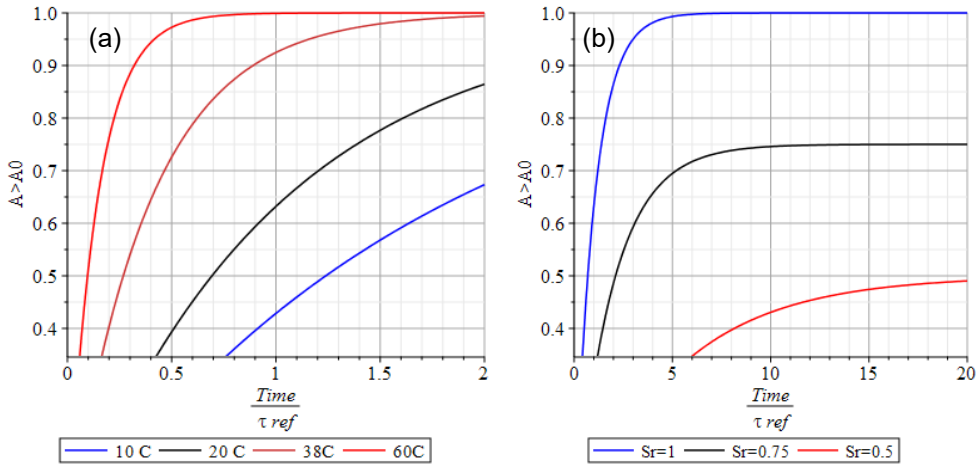

Figure 3.4: (a) Influence of temperature with $Ea = 40kJ/mol$, (b) Influence of the water saturation rate (Sr) on the chemical kinetic and on the amplitude of AAR advancement ($\bar{S}_r = 0.1, A_0 = 0.35$) using equations (7) and (8)

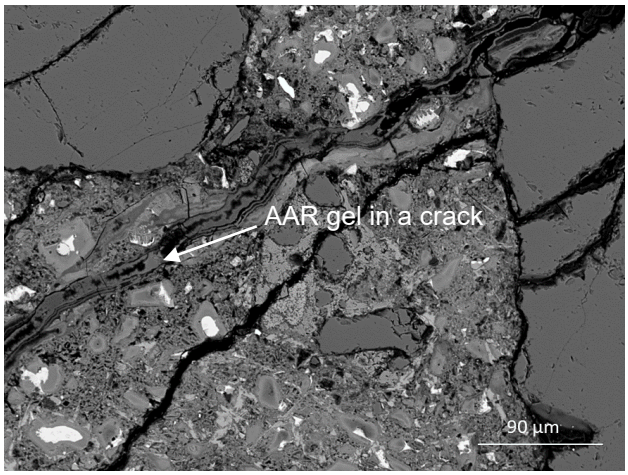

Figure 3.5: AAR gel in a micro-crack (SEM picture kindly provided by S.Feldman from NIST, 2018)

3.1.2 Delayed ettringite formation (DEF)

Concerning DEF, the thermodynamic chemistry framework explains well the cycle of ettringite, with the dissolution process at high temperature and the delayed re-precipitation at ambient temperature [34]. This phenomenon is the consequence of the dependence of the solubility constant of ettringite (K in equation 12) towards the temperature. This dependence can be considered using a classical Van't Hoff law, which traducts the fact that ettringite solubility increases with the temperature (equation 12 is illustrated in Figure 3.6). When the ionic product (Q in equation 11), is such that the crystallisation

pressure (P in equation 10) is reached, the crystallisation occurs [35]. Figure 3.6 shows that the ionic activities product must be ten thousand times greater at 80°C than at 20°C, explaining the facility to dissolve ettringite at this temperature, such temperatures were sometimes reached in the past, during the hydration of massive structures, before the standards limit the temperature in massive structure at early age [36].

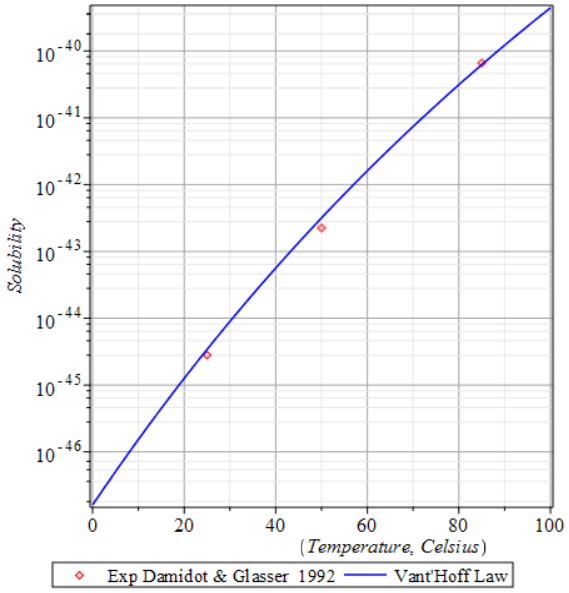

Figure 3.6: Solubility of ettringite versus temperature, experimental results (points) from [37], Vant'Hoff law (line) with $K^0 = 1.25e-45, \Delta H_r^0 = 145 kJ/mol$

Structural problems induced by DEF occur during the reprecipitation stage, at low temperature, when secondary ettringite has not enough space to precipitate and crystallize under pressure. As the main components of ettringite come from cement paste, the crystallization occurs first into the paste which swells first, leading to a debonding at cement paste-aggregate interfaces. The ettringite can then precipitate in the voids created at the interface as illustrated in Figure 3.7. As the tensile strength of the interface is better for lime aggregates then for silica ones, the concretes made with siliceous aggregates are more sensitive to the DEF. This was confirmed experimentally, for instance in Malbois, Divet, Lavaud and Torrenti in [17] (p.106). If the precipitation zone is tight, the crystallisation pressure increases, leading to massive deleterious ettringite. If later, due to the cracking of cement paste, the pressure decreases, a part of delayed ettringite may dissolve again due to the crystallization pressure decrease and re-precipitates in lower pressure zones, for instance in the voids created at the cement-paste-aggregate interfaces, as illustrated in Figure 3.7.

$$6\,Ca^{2+} + 2Al(OH)_4^- + 3SO_4^{2-} + 4(OH)^- + 26H_2O \leftrightarrow \text{Ettringite (Aft)} \tag{9}$$

$$P = \frac{RT}{V} \ln\left(\frac{Q}{K}\right) \tag{10}$$

$$Q = (Ca^{2+})^6 (Al(OH)_4^-)^2 \left(SO_4^{2-}\right)^3 (OH^-)^4 \tag{11}$$

$$\ln(K) = \ln(K^0) + \frac{\Delta H_r^0}{R}\left(\frac{1}{T^0} - \frac{1}{T}\right) \tag{12}$$

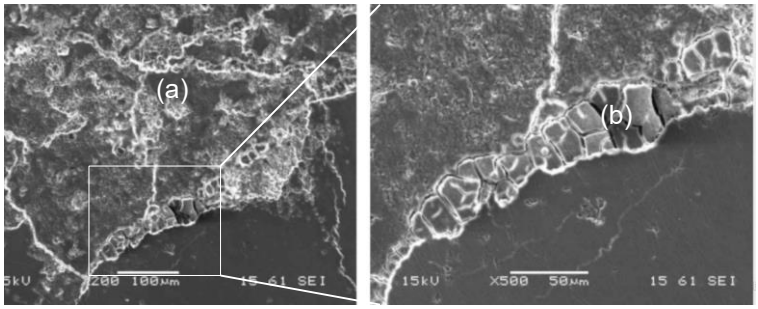

Figure 3.7: (a) crystallisation of delayed ettringite in cement paste, (b) crystallisation of massive ettringite in debonded zone at the cement past-aggregate interface (SEM pictures from LMDC & C.Noret and K Lachiche in [17], p.295)

The experimental evidences of a pessimum in terms of heating cycles duration and amplitude are given in [5]. The phenomenological modelling provided in IFSTTAR's works [38] shows that DEF is maximal if the temperature threshold allowing the primary ettringite dissolution is maintained during an optimal period. The explanation of this optimal period was proposed by Salgues et al. in [39], who, using a thermodynamic data base, showed that during the high temperature period, aluminate released by dissolved primary ettringite could be combined to C-S-H to form Hydrogarnet [40], thus depriving the pore solution of Aluminium (needed for secondary ettringite formation). Finally, the pessimum existence can be summarised as follows: If the heating cycle is too short, sulphates and aluminates stay in primary hydrates, while, if the heating cycle is too long, the aluminates are captured by C-S-H and no more available to form secondary ettringite.

As chemical thermodynamic models are non-linear and involve numerous chemical species they are too heavy (in terms of numerical methods) to be used as "subroutines" in a mechanical finite element models usable at structural scale. That is the reason why the main phenomena of the DEF were summarised in a lighter chemical model compatible with structural modelling [41]. In this simplified model tree kinetics are in competition:

- The dissolution of sulfoaluminates phases (equation 9) if the temperature exceeds a threshold $T_{th,d}$ depending on alkali content (Figure 3.8).
- The fixation of aluminium in Hydrogarnet (equation 10) if the temperature exceeds a second threshold $T_{th,f}$, in order to consider the pessimum of heating cycles
- The precipitation of delayed ettringite (equation 13) if the temperature is lesser than the first dissolution threshold $T_{th,d}$.

$$\frac{\partial(AFt + AFm)}{\partial t} = -\frac{AFt + AFm}{\tau^d} \tag{13}$$

In equation (13) AFt is the moles number of ettringite, AFm the monosulfoaluminate moles number, τ^d the characteristic time for the dissolution of sulpho-aluminates when the temperature exceeds $T_{th,d}$ (equation 14 and Figure 3.8).

$$T_{th,d} = T_{th,d}^{ref}\left(\frac{\overline{Na}^+}{\widetilde{Na}^+}\right)^n \text{ with } \widetilde{Na}^+ = max(Na^+, \overline{Na}^+) \tag{14}$$

In equation 14, a fitting on Brunetaud experimental results [42], [43], leads to $T_{th,d}^{ref}$=80°C, $\overline{Na}^+ = 0.28\, mol/l$ and $n = 0.19$. This equation shows that higher the alkali content lowers the dissolution temperature of sulpho-aluminates.

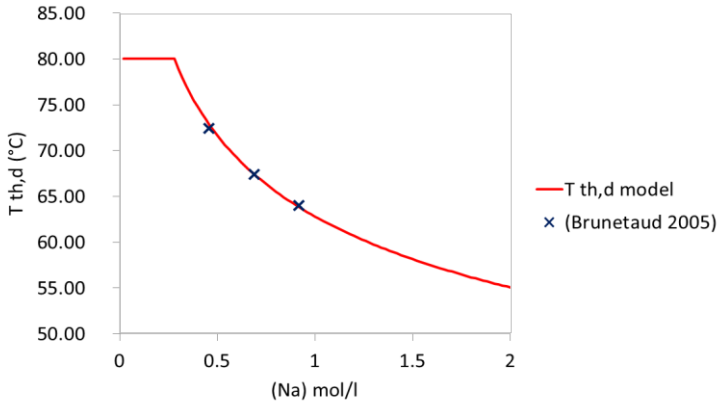

Figure 3.8: Influence of alkali concentration in water on threshold temperature of ettringite dissolution, from experimental results of Brunetaud [42], [43] and modelling provided by [38], [41].

$$\frac{\partial \tilde{A}}{\partial t} = -\frac{\partial (AFt + AFm)}{\partial t} - \frac{\partial HG}{\partial t} - \frac{\partial DEF}{\partial t} \tag{15}$$

In equation 15, $\tilde{A}$ is the mole number of aluminium released in the pore solution, it is the consequence of the dissolution (eq. 9) and of the fixation processes, either in Hydrogarnet at high temperature (HG in eq. 15), or in delayed ettringite at low temperature (DEF in eq. 15).

$$\frac{\partial HG}{\partial t} = \frac{\tilde{A}}{\tau^f} \tag{16}$$

In equation (16), τ^f is the characteristic time of fixation of aluminium in Hydrogarnet (HG). To compute the maximal amount of realizable DEF (DEF_∞ in eq. 18), the sulfate moles number in solution $\tilde{\tilde{S}}$ must be known, that is the reason why equation (17) is used. In (17) K^1 and K^2 are stoichiometric constants and A^1 the alumium moles number in hydration products (depending on the cement composition).

$$\frac{\partial \tilde{\tilde{S}}}{\partial t} = -K^1 \frac{\partial A^1}{\partial t} - K^2 \frac{\partial DEF}{\partial t} \tag{17}$$

In (18) τ^p is the characteristic time of precipitation, depending on the alkali content in pore solution (Na^+) of concrete through the equation (19), and leading, as illustrated in Figure 3.9, to a reduction of kinetic of the DEF in case of high alkali content. This phenomenon is explained by the sulphate binding capacity of C-S-H which increases with the alkaline concentration in water, as shown by Divet et al. in [44]. This is also why alkaline leaching is recommended to speed up DEF testing, and why in structures affected by both AAR and DEF, DEF only begins when AAR has consumed a significant portion of the alkalis, as observed in [45].

$$\frac{\partial DEF}{\partial t} = \frac{1}{\tau^p}\left(DEF_\infty - DEF\right) \tag{18}$$

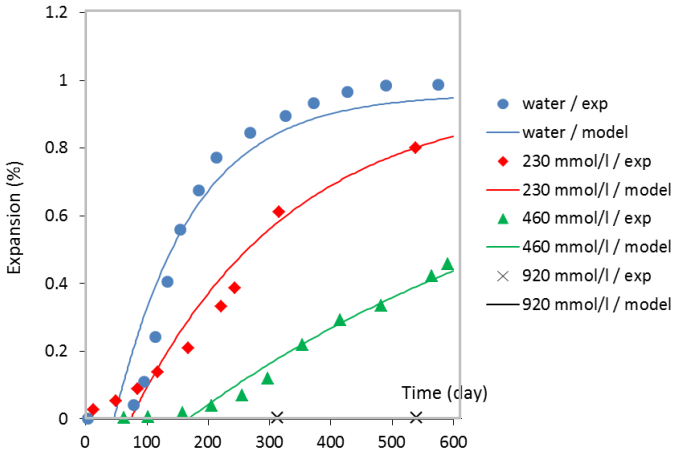

Figure 3.9: Influence of alkali concentration in water on DEF kinetic, experimental results from [44], and modelling from [41].

As water is a component of DEF and allows the diffusion of chemical species, the kinetics of DEF have a greater dependence on concrete moisture than AAR, as illustrated in Figure 3.10 where the influence functions of water acting on AAR and DEF respectively are compared. It is clear that DEF needs a higher saturation ratio than AAR to occur; in fact, near-saturation is required to have half of the maximum def kinetics (very close to saturation), while the same rate is achieved for AAR at 75% of water saturation.

$$\tau^p = \tau^p_{ref}\left(exp\left(-\frac{1-S_r}{1-\bar{S}_r}\right)\left(H(Na^+ - \overline{Na}^+)\left(\frac{\overline{Na}^+ - Na^+}{\overline{Na}^+}\right)^m\right)C_p^T\right)^{-1} \quad (19)$$

With regard to the characteristic weather of precipitation, т-p. the connection made in [41] leads to m= 3, $\overline{Na}^+$=0,92mol/l, C_p^T is a thermal coefficient combining the thermal activation of the DEF at moderate temperature with the effect of the dissolution temperature threshold at higher temperatures, it is detailed in [41].

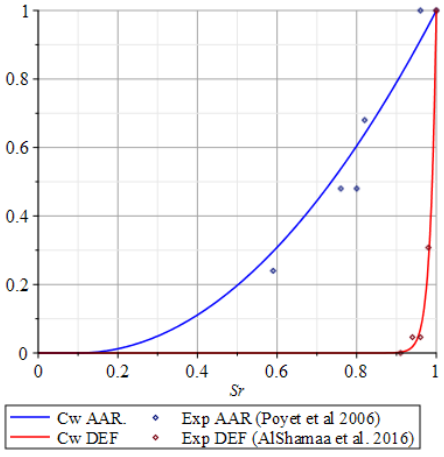

Figure 3.10**:** Influence of water saturation ratio (Sr) on normalized kinetic for AAR (in blue) and DEF (in red); models correspond to eq.8 for AAR (with $\bar{S}_r$=0.1) and to eq. 19 for DEF (with $\bar{S}_r$=0.95). Experimental points are deduced from swelling tests at controlled HR performed by Poyet et al. for AAR and from Al Shamaa et al. for DEF [19], [45]

To close this first section, devoted to the simplified chemical modelling of the main phenomena encountered in SRI, it can be noted that even if many experimental phenomena are generally well

understood, their modelling remains a challenge because the models must take into account temperature and humidity, but also other parameters capable of limiting the reaction (such as the formation of hydrogarnet at high temperature in case of DEF), or to change the composition and texture of products (such as calcium which tends to crystallize the AAR gel), all under the constraint of a limited numerical blow. Despite their limitations, these types of models are the starting points for the chemo-mechanical modelling described below.

3.2 Meso-scale and interactions between aggregates and cement paste

3.2.1 Chemical aspects at meso scale

Concerning AAR, the origin of the pessimum relative to the reactive aggregate size was explained by a meso-scale diffusion model initially proposed in [28], [46]. The principle consisted to homogenize the alkali diffusion flow from paste to the aggregates as a source term included in the mass balance equation of alkali used in the cement paste surrounding the aggregates; this method is close to the self-consistent scheme often used in homogenization theory. The method was recently enhanced by S.Multon et al. in [47], who added the influence of an alkali threshold for the dissolution stage of reactive silica in the aggregates. In their model, the AAR gel, created in the sand and small aggregates, migrates to the porosity of the cement paste without damaging the paste, while the gel produced in large aggregates cannot be fully absorbed by the paste surrounding it; so the gel largely remains in place, its pressure rises, which damages the aggregates and the surrounding paste; it is then common to observe that the AAR gel migrates into the cracks thus created, as illustrated in Figure 3.5; That is the reason why only the cracking induced by the “large” aggregates leads to a significative concrete swelling. For very large aggregates the time needed by alkali to reach reactive silica pockets disseminated into these aggregates is so long that the final swelling cannot be reached at human time scale, while, for sand and smaller reactive particles, the diffusion time is reduced but the effects are negligible in terms of damage and swelling due to the gel migration in connected porosity. An example of pessimum curve relative to the aggregates sizes is given in Figure 3.11 (b) where it is compared to the mesoscopic chemical model [47].

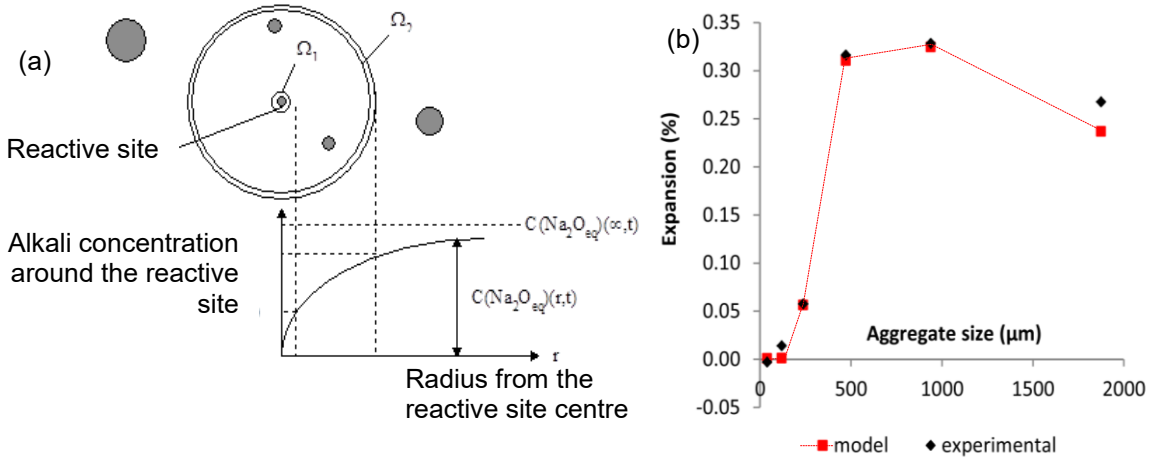

Figure 3.11: (a) Chemical homogenization principle to consider alkali diffusion from paste to the aggregates (scheme adapted from [28]), (b) pessimum effect of reactive aggregate size (scheme adapted from [47]).

Concerning DEF, the interest of chemical meso-scale modelling is lower if the crystallization pressure is not considered because the main phenomena start at nano and micro-scale, in the cement paste, as explained in section 3.1.2. Therefore, some authors resorted to chemical micro diffusion to explain spalling of specimens affected by external sulphate attacks and AAR [48]. This phenomenon is more due to the influence of boundary condition than to the fact that aggregates are considered in the model as illustrated in Figure 3.12. But this type of model would benefit from being improved by allowing the ettringite precipitated in the cement paste to re-dissolve, and to reach the aggregate/paste interfaces damaged by the swelling of the cement paste. Such modelling is not easy because it is necessary to model the debonding between aggregate and paste, the pressure of dissolution ettringite, the diffusion

of dissolved species, and the reprecipitation of ettringite in zones of lower pressures; a beautiful chemo-mechanical problem not yet solved !

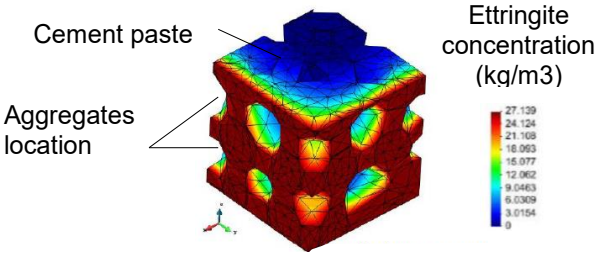

Figure 3.12: Ettringite precipitation simulated with the model developed by Carol, Liaudat and Lopez (illustration adapted from [17] pp248-260).

3.2.2 Mechanical aspects at meso-scale

3.2.2.1 Interest of numerical simulations at meso-scale

As mentioned above, the interaction between paste and aggregates is of primary importance to understand the mechanical effects of AAR and DEF. Figure 3.13 is an illustration of a micro-mechanical model proposed by Giorla, Dunant and Scrivener in [9]. This model was in two dimensions for sake of computational duration, what limits its scope. However, the interest of this type of modelling is to help understanding the cracking phenomena at meso-scales. An interesting conclusion of their paper [9], is that cement paste could absorb a part of aggregate's swelling before cracking if its creep rate allows it. Indeed, in this modelling, the only way to avoid overestimating of the swelling caused by the cracking of the cement paste due to the expansion of the aggregate was to use a creep model of the cement paste. Another explanation would be to let some of the gel migrate to the cracks in the cement paste, and to the porosity surrounding the aggregates, but the authors did not assume this, as they worked with aggregates in which the reactive silica is meso-dispersed in concentrated pockets inside the aggregates, leading to gel pockets that first damage the aggregates, then crack the cement paste in a second time without the gel being able to migrate into the cracks thus created. When reactive silica is homogeneously distributed in the aggregate (micro-dispersed or massive) a ring of damaged aggregate can appears as shown in Figure 3.1 (a). Other topologies of reactive silica (like veins) can lead to other damage patterns. Finally, micro mechanics analysis combined with SEM observations show that macroscopic swelling of concrete subjected to the AAR is mainly due to the cement paste cracking under the effect of the pressure induced by the swelling of reactive aggregates (and the gel it contains); and whatever the underlying topology of reactive sites in the aggregates, the main problem to solve in order to predict macroscopic swelling, is the multi-cracking of the cement paste due to the aggregate's swelling, and in some cases the migration of gel from aggregate to the cracks. Finally, the meso-scale modelling shows that the capability of cement pastes to absorb a part of aggregate's swelling before cracking can play a non-neglectable role (either by creep of the cement paste, or allowing the gel migration to its porosity, or the both), it shows also that without cracking inside and/or around aggregates, swelling would be limited. So, it is necessary to consider these phenomena with attention when dealing with mechanical effects of swelling reactions.

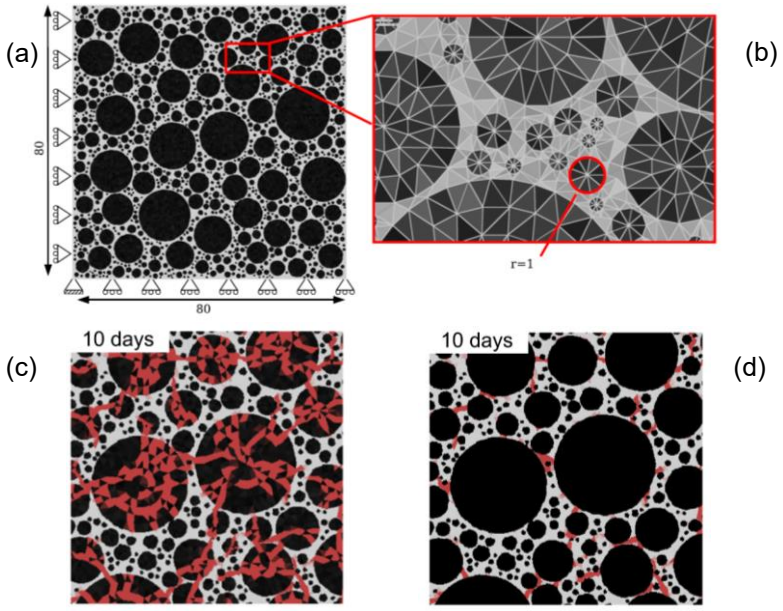

Figure 3.13: Illustration of the 2 dimensional modelling proposed by Giorla, Dunant and Skrivener to explain the crack propagation from reactive sites pocket inside the aggregates until the cracking of the paste; (illustration adapted from [9] and pp. 144-160 in [17])

In Figure 3.13, (a) is the 2D mesh of a representative elementary volume with aggregates in black, (b) is a zoom on aggregate's mesh, (c) represents in red the damage inside the aggregates, and (d) is damage to cement paste, which connects the swelling aggregates.

3.2.2.2 Analytical modelling of mechanical behaviour at meso-scale

In order to highlight the importance of micro-mechanic's phenomena occurring at meso-scale, a criterion based on stresses concentration at cement paste-aggregate interfaces can be used [49]. For this purpose, the stress field around aggregates has to be expressed analytically. In case of swelling of the aggregate an orthoradial stress concentrations occurs (for instance σ_{zz} symbolized by the green arrows and red fields in Figure 3.14). In absence of external loading these stresses are maximal at the interface between swelling aggregates and cement paste, and decrease as the inverse of radius square (axe x or y in Figure 3.14). The cracking starts in the cement paste when the orthoradial tension (σ_{yy} or σ_{zz} in Figure 3.14) reaches the tensile strength of the cement paste at the interface.

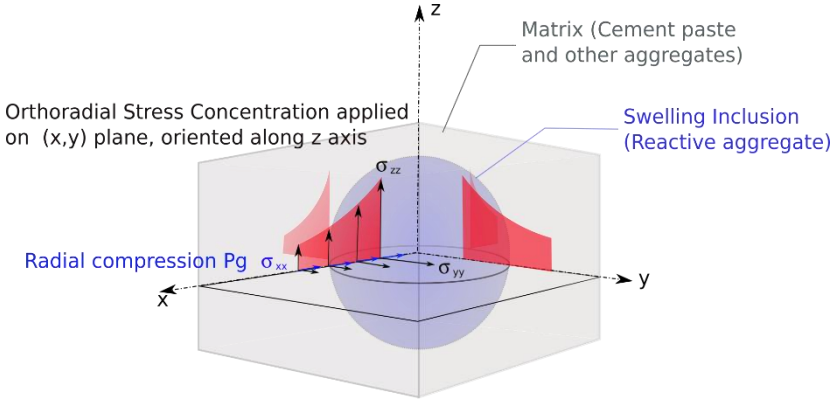

Figure 3.14: Orthoradial tensile stress concentrations around spherical swelling (σ_{yy} and σ_{zz} are orthoradial tension induced by the swelling of the aggregate, while $\sigma_{xx}$is the pressure applied by the aggregate on the matrix)

After solving of local equilibrium equations and considering the elastic behaviour of aggregates and matrix in one hand and a homogenization scheme in the other hand (Mori Tanaka scheme in this case [50]), the pressure applied by the swelling aggregate on the matrix is given by equation (20), this pressure corresponds to the blue arrows in Figure 3.14. In equation (20) ε_z^g is the free directional swelling (strain) of the aggregate due to the AAR. Km, Gm, Ki, Gi are respectively the bulk modulus and shear modulus for the matrix (index m) and for the inclusion (index i). φ is the volume fraction of reactive aggregates in the concrete.

$$P^g = \frac{12(1-\varphi)Ki.Gm.Km.\varepsilon_z^g}{4\big((1-\varphi)Km + \varphi.Ki\big).Gm + 3.Ki.Km} \quad (20)$$

The value of ε_z^g can be deduced from chemical models at micro and meso scales described above. For instance, if the gel produced by the AAR does not migrate to the cement paste, a proportionality of aggregate swelling to the reaction advancement can be adopted (equation 21).

In equation (21) $\Delta\varphi^{g\infty}$ is the volume change of aggregate due to the total achievement of AAR, A the advancement rate of the reaction given by equation (7), and A_0 the chemical advancement threshold for which the swelling of the aggregates starts (as illustrated in Figure 3.2).

$$\varepsilon_z^g = \frac{1}{3}(A - A_0)\Delta\varphi^{g\infty} \quad (21)$$

The orthoradial tensions illustrated in Figure 3.14 can be assessed by the micro-mechanic analysis; its expression is given by relationship (22) in the framework of linear mechanics. It is also possible to assume that a part of the gel migrates to the cement paste porosity; in this case the term ε_z^g must be reduced, considering only the residual gel staying in the aggregate, this assumption was used for instance by Grimal et al. [51] or Morenon et al. in their structural model [52].

$$\sigma_{zz}^{g/Pg} = \frac{6(2\varphi + 1)Km.Ki.Gm.\varepsilon_z^g}{4\big((1-\varphi)Km + \varphi.Ki\big).Gm + 3.Ki.Km} \quad (22)$$

Expressions (20) and (22) allow expressing the ratio Cg (equation 23), between the orthoradial stress concentration around the swelling aggregate $\sigma_{zz(r=R)}^g$ and the radial pressure P^g applied by the aggregate to the matrix. This ratio is independent of the pressure and of the elastic properties of matrix and inclusions; In the framework of linear mechanics it depends only on the volume fraction of swelling aggregates φ (equation 23).

$$Cg = \frac{\sigma_{zz}^{g/Pg}}{P^g} = \frac{2\varphi + 1}{2(1-\varphi)} \quad (23)$$

The evolution of Cg versus the fraction of swelling aggregates is given in Figure 3.15 (a). It starts from 0.5 for a low concentration of reactive aggregates and tends to the infinity when the volume fraction of reactive aggregates tends to the unit. For a volume fraction varying from 20% to 50% the stress concentration factor varies from 1 to 2. It is a relatively stable value interesting to keep in minds when simplifications have to be done to clarify macroscopic models, as explained in the third section bellow.

(a) stress concentration factor Cg for the swelling pressure

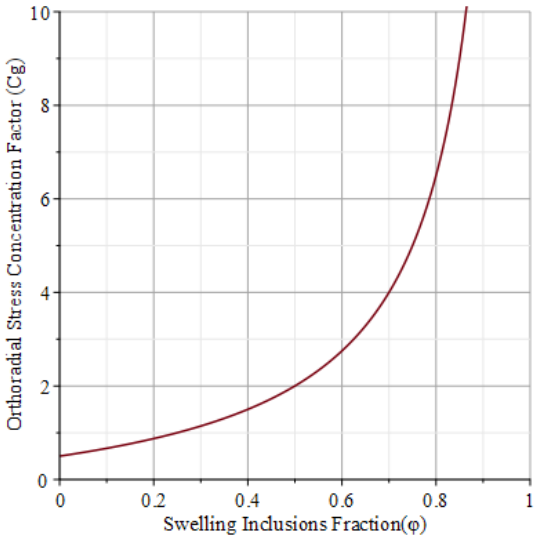

Figure 3.15: (a) Stress concentration factor of the orthoradial stress induced around a swelling inclusion by the swelling pressure and (b) by the external uniaxial loading

The linear micro-mechanics allows also assessing the effect of an external loading in the vicinity of the aggregate. The expression of the stress concentration factor Cs, linking the external loading in vertical direction at the infinity (σ_{zz}^{∞}) and the local tangential stress at the inclusion-matrix interface in the vertical direction ($\sigma_{zz}^{g/\infty}$) is relatively complex in general cases, but simplifies in equation (24) if the Poisson ratio $\upsilon = 0.2$, which is the usual value adopted for concretes. As shown by equation (24), the external loading concentration factor Cs depends on the volume fraction of reactive inclusions φ, and on the Young moduli ratio between inclusions and matrix (Ei, Em) respectively. A typical value of Cs is between 0.5 and 1; Note that *Cs* can evolve during the AAR due to the cracking of the reactive aggregates or/and of the matrix. If, for instance, the initial Young modulus of the aggregate is twice the matrix one, and if the aggregate damages to reach the matrix one, *Cs* increases from 0.5 to 1. It means that the effect of aggregate's damage leads to an increase of external loading effect, but, in the other hand, the damage of cement paste decreases *Cs* because if Em decreases, Cs also. that is a reason why it is so difficult considering properly the effects of external loadings on swelling mitigation.

$$Cs = \frac{\sigma_{zz}^{g/\infty}}{\sigma_{zz}^{\infty}} = \frac{2\,Em}{(Ei - Em)\varphi + (Ei + Em)} \tag{24}$$

As, in case of AAR, the main cause of concrete swelling is the matrix cracking, and as matrix cracking starts when the tangential stress at the aggregate-matrix interface exceeds the tensile strength of the matrix (Rt in equation 25), the cracking condition of the cement matrix can be summarized by the directional (anisotropic) criterion (25).

$$f_{zz}^{g} = \sigma_{zz}^{g} - Rt > 0 \quad \text{with} \quad \sigma_{zz}^{g} = \sigma_{zz}^{g/Pg} + \sigma_{zz}^{g/\infty} \tag{25}$$

Using the stress concentration factors Cg and Cs defined above allows expressing the cracking criterion ($f_{zz}^{g} > 0$) directly as a function of the swelling pressure P^{g} and of the external loading applied to the concrete σ_{zz}^{∞}.

$$f_{zz}^{g} = (Cg.P^{g} + Cs.\sigma_{zz}^{\infty}) - Rt > 0 \quad (26)$$

This type of micro-mechanics criterion (26) was proposed first in 2002 in [23], (in a simplified version for which Cg=Cs=1) and adopted next to develop the models implemented in "Code-Aster", the finite element code of EDF [12], [39], [53], [54]. This criterion is anisotropic, it allows finding the external stress able to block the micro-cracks propagation in the matrix in the planes perpendicular to the compressed direction. It corresponds to the expression of σ_{zz}^{∞} which cancels the cracking criterion f_{zz}^{g}. With the same assumptions than for equation (24) (i.e Poisson ratio equal to 0.2), the external vertical stress able to block cracking in the horizontal plane simplifies and becomes equation (27).

$$\sigma_{zz}^{\infty} = \left(6(\varphi + 1)\, Rt - 10\, Em\, \varepsilon_{z}^{g} \left(\varphi + \frac{1}{2}\right)\right) \frac{1}{12}\left(\frac{Ei}{Em}\right) - \left(Rt\, \frac{\varphi - 1}{2}\right) \quad (27)$$

The external "blocking stress" σ_{zz}^{∞} (27) is valuable in the particular case of a uniaxial loading along z axis. To illustrate the results of this micromechanics analysis, the evolution of the vertical "blocking stress" σ_{zz}^{∞} avoiding the crack propagation on the x-y plane (and then the swelling in direction z), is plotted in Figure 3.16, versus the aggregate imposed unidirectional swelling ε_{z}^{g}. The plot is done with a Young modulus of 20GPa for the matrix, 4GPa for the gel and a tensile strength of 3MPa for the matrix. The gel production rate of the aggregate occupies a volume ($\varphi = 3.\varepsilon_{z}^{g}$) which varies from 0 to 1% (corresponding to an axial swelling of reactive spots of 0.33% in the vertical direction).Note the theoretical stress able to ovoid vertical swelling is, for this example, close to the empirical law proposed by Charlwood in [1], who estimated the value to 5 MPa.

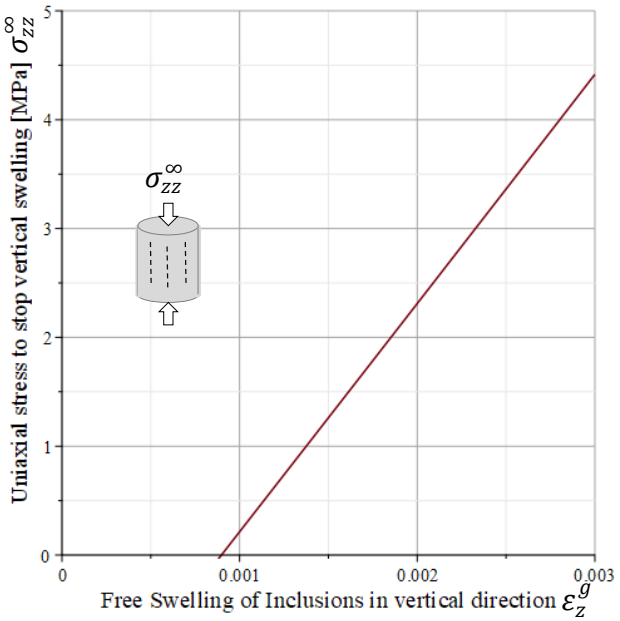

Figure 3.16: Theoretical stress able to avoid vertical swelling in case of uniaxial loading, versus free swelling of AAR gel spots (Ei=4GPa, Em=20Gpa, $\varphi = 3\ \varepsilon_{zz}^{g}$)

Another interesting result of micromechanics analysis is the prediction of the blocking stress in cases of tri-axial loadings. This problem is of great interest for the modelling of massive structures where swelling concrete is confined. Using the same assumptions than above (Poisson coefficient equal to 0.2 for both the matrix and the aggregates), and assuming a radial applied pressure at structure level p, the axial "blocking stress" can be computed using the same cracking criterion than above (equation 25); it leads to expression 28, in which the radial pressure p modifies linearly the vertical "blocking stress"; higher the radial pressure p, higher is the vertical stress needed to block axial swelling. An illustration of the radial confinement effect on the axial "blocking stress" is given in Figure 3.17.

$$\sigma_{zz}^{lb} = \frac{\left(\left(-10\, g\, \varphi\, -\, 5\varepsilon_{zz}^{g}\right)Ei\, +\, 6(1-\varphi\,)Rt\, -\, 3p\right)Em\, +\, 3Ei(2(\varphi+1)Rt\, +\, p)}{12Em} \tag{28}$$

The consequence of this analysis is a dependence of the swelling reduction rate versus the radial external pressure as illustrated in Figure 3.17 (b). As seen below, this effect was detected by engineers dealing with structural analysis who consider empirically this effect modifying the Charlwood's law. For instance Goveski and Yildis proposed to use a larger axial stress in case of confinement in [17] p.196, and Saouma et al. use empirical functions to reduce swelling in case of multiaxial loading [3]. To avoid using empirical laws, Grimal et al. use directly the anisotropic cracking criteria (equation 26) in their structural models, but assumed constant values for stress concentration factors *Cg* and *Cs* for sake of simplicity [22]. The model of Grimal et al. was used recently by Morenon et al. [55] to explain experimental results of swelling in triaxial cells performed by Liauda [4].

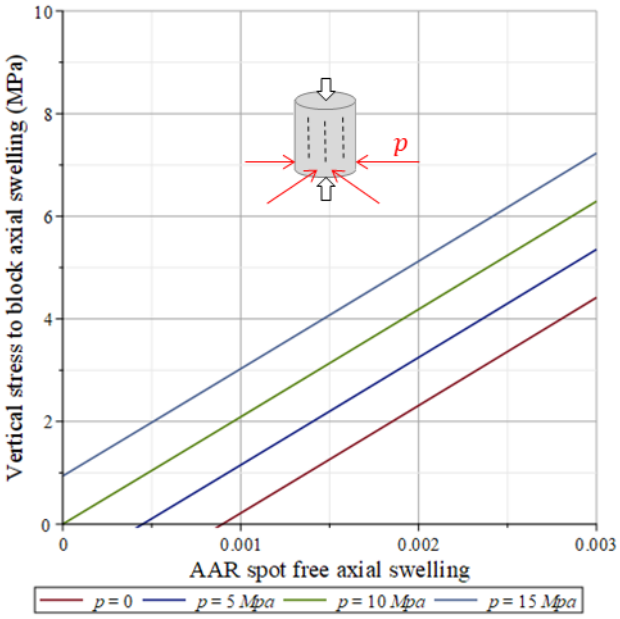

Figure 3.17: Theoretical axial stress to block vertical swelling versus AAR spot axial swelling for (Ei=4GPa, Em=20Gpa, $\varphi = 3\,\varepsilon_{zz}^{g}$)

3.3 Modelling swelling effects at structural scale

3.3.1 Modelling swelling anisotropy at structural scale

As mentioned in the introduction, the main issue dealing with structural effects of AAR and DEF is to predict concrete's swellings and damages. In a complex structure like a reinforced concrete bridge, or a dam (Figure 3.18 a), the stress state depends on external loadings and, also, on boundary conditions which avoid swellings but create stresses sometimes dangerous for the basements of the structure. It is then needed to predict the interactions between macroscopic stresses and swellings. The complexity of this problem comes from the fact that swellings depend themselves anisotropically on the stress state, as demonstrated in last section by resorting to micro-mechanics. So, in real structures there is a coupling loop, illustrated in Figure 3.18 (b), which controls anisotropy and amplitude of swellings, of damages, of stresses and observed displacements.

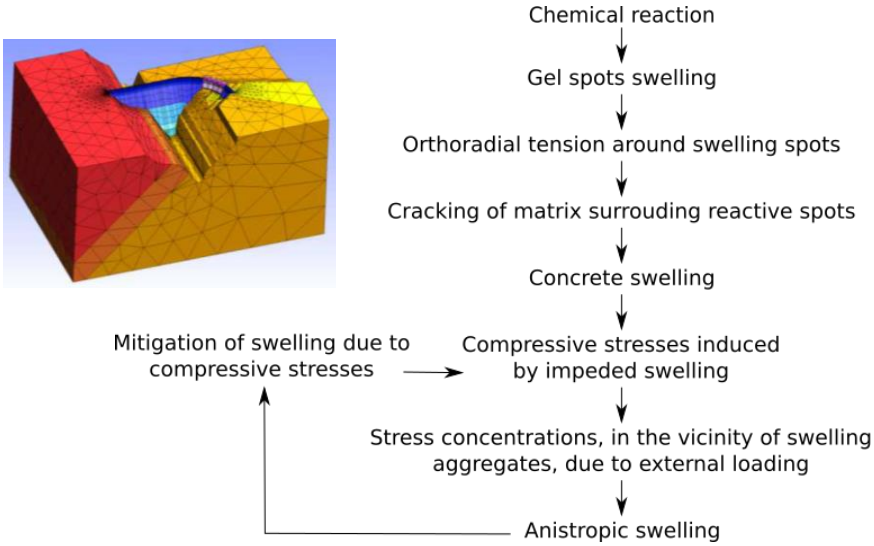

Figure 3.18: Coupling loop between swelling at meso scale and boundary conditions leading to anisotropic swelling of concrete (illustration Chambon dam studied by Grimal et al. [56]).

The first method used to consider the capability of compressive stresses to mitigate swelling was proposed by Charlwood [1]. Is was an empirical law, fitted on unidirectional observations, decreasing the imposed swelling rate versus the axial stress as explained in the last section. Later the method was generalized in three dimensions by Saouma et al., using several interpolation functions to reduce swelling versus the three-dimensional stress state [3]. In last, the microstructural based criteria corresponding to equation (26) were used by Morenon et al. in [55] in the context of plasticity coupled to damage mechanics, but, until now, only with constant stress concentration factors (*Cg* and *Cs* in equation (29)). Therefore, this combination of theories allows to consider deleterious effects of cracking on concrete stiffness trough the damage theory, and the possibility of plasticity or creep induced by loading. To achieve this coupling, the external stress $\sigma_{zz}^{\propto}$ used in (26) is replaced in equation (29) by the stress in undamaged zones noted ($\tilde{\sigma}_{zz}^{\propto}$) and deduced from the last using the damage theory : $\tilde{\sigma}_{zz}^{\propto}(1 - D_{zz}^{g}) = \sigma_{zz}^{\propto}$, with D_{zz}^{g} the damage induced by the propagation of microcracking.

$$f_{zz}^{g} = (Cg.P^{g} + Cs.\tilde{\sigma}_{zz}^{\infty}) - Rt > 0 \tag{29}$$

Concerning the swelling pressure at reactive aggregate's scale (P^{g} in equations 26 and 29), it is assessed in the framework of poro-mechanics, what allows considering the chemical advancement *A* and the modification of concrete porosity connected to the reactive spots induced by the concrete deformation (tensor $\bar{\bar{\varepsilon}}$ in equation 30). In equation (30), the swelling at aggregate's scale (φg) is compared to the capability of concrete to absorb the reaction products ($\emptyset vg$). If the pressure (30) allows the criteria (29) to be reached, that provokes a plastic strain $\bar{\bar{\varepsilon}}^{pg}$, decreasing the gel pressure Pg to verify the criteria.

$$\frac{P^{g}}{M^{g}} = \underbrace{(A - A_0)\varphi^{g\infty}}_{\varphi g} - \underbrace{\left(P_{max}^{g}\frac{\varphi_0^{g}}{Rt} + b^{g}tr(\bar{\bar{\varepsilon}} - \bar{\bar{\varepsilon}}^{pl} - \bar{\bar{\varepsilon}}^{pg}) + tr(\bar{\bar{\varepsilon}}^{pg})\right)}_{\emptyset vg} \tag{30}$$

In equation (30) several phenomena are considered: first the chemical aspect with *A, A0* and $\varphi^{g\infty}$ which have the same definitions than in equations (4-5, cf. chemical section above). Secondly the interactions with the concrete matrix through φ_0^{g}, which considers the possibility for the AAR gel to migrate from the reactive aggregates to the connected porosity of the cement paste. The term $b^{g}tr(\bar{\bar{\varepsilon}} - \bar{\bar{\varepsilon}}^{pl} - \bar{\bar{\varepsilon}}^{pg})$ considers the effect of the concrete matrix deformation, and the term $tr(\bar{\bar{\varepsilon}}^{pg})$ considers the possibility for the gel to migrate into the micro cracks induced by aggregates swelling

(as illustrated in Figure 3.5). M^g is the Biot modulus of the gel in interaction with the matrix, b^g is the Biot coefficient [57]. The micro-mechanics allows linking these poro-mechanics coefficients to the volume change of reactive phases φg : Equation (31), also used in [41], and build with a Poisson ratio of 0.2, links the Biot coefficent b^g to φg , and equation (32) links b^g with the Biot Modulus M^g.

$$b^g = \frac{(3\,Km\,\varphi g\ +\ 4\,Gm)Kg}{\varphi g\,(-3\,Kg\,\varphi g\ +\ 3\,Km\,\varphi g\ +\ 4\,Gm\ +\ 3\,Kg)} = \frac{2\varphi g}{1+\varphi g} \text{ if } \upsilon = 0.2 \tag{31}$$

$$\frac{1}{M^g} = \frac{b^g - \varphi g}{K^s} + \frac{\varphi g}{K^g} \tag{32}$$

With $\mathrm{K^s}$ the bulk modulus of concrete linked to its Young modulus E and Poisson ratio υ by equation 33, $\mathrm{K^g}$ the bulk modulus of the AAR gel spots.

$$K^s = \frac{E}{3(1-2\upsilon)}\frac{1}{(1-b^g)} \tag{33}$$

In equation (30), $\bar{\varepsilon}^{pl}$ is a deformation tensor accounting for the localized structural cracks, and $\bar{\bar{\varepsilon}}^{pg}$ the tensor of deformations corresponding to the micro cracks induced by AAR. Therefore, the model is able to consider simply the coupling loop illustrated in Figure 3.18 (b). In fact, the evolution of $\bar{\bar{\varepsilon}}^{pg}$ is controlled only by equation (29) by means of a classical associated plastic flow method (equation 34).

$$\frac{\partial \varepsilon_I^{pg}}{\partial t} = d\lambda_I \frac{\partial f_I^g}{\partial \tilde{\sigma}_I} \tag{34}$$

In (34) $d\lambda_I$ are the plastic multipliers allowing to return to $f_I^g = 0$ (cf. equation 29) if f_I^g was postive after a step of chemical evolution dA, or a step of mechanical loading $d\bar{\bar{\varepsilon}}$. The combination of equations (29 to 34) allows computing these plastic multipliers. As this formulation is based on criteria expressed in the principal direction of stresses ($\tilde{\sigma}_I\ = \sigma_{zz}^{\propto}$ in equation 29), the tensor $\bar{\bar{\varepsilon}}^{pg}$ becomes naturally anisotropic in case of anisotropic loading ($\tilde{\sigma}_I\ > \tilde{\sigma}_{II} > \tilde{\sigma}_{III} \rightarrow d\varepsilon_I^{pg} > d\varepsilon_{II}^{pg} > \varepsilon_{III}^{pg}$), , avoiding resorting to empirical laws to modulate the swelling rate versus the principal directions of stresses, like it was the case in previous AAR structural models [1], [58], [59].

3.3.2 The importance of concrete creep

AAR is a long-term phenomenon, so the structures can deform by creep during AAR. As shown in Figure 3.19, the creep amplitude of concrete cylinders under 10 MPa compressions (-0.1%) is of the same order than the AAR free swelling (between +0.1%). More, in accordance with the phenomena explained in previous sections, the swelling is reduced in compressed directions and amplified in free directions (see for example Figure 3.19 (b) specimen under 20MPa compressive stress). So, the error neglecting the concrete creep is of the same order than if AAR swelling was neglected. That is the reason why several experimental programs try, now, to quantify creep and AAR interactions [8], [60]–[62].

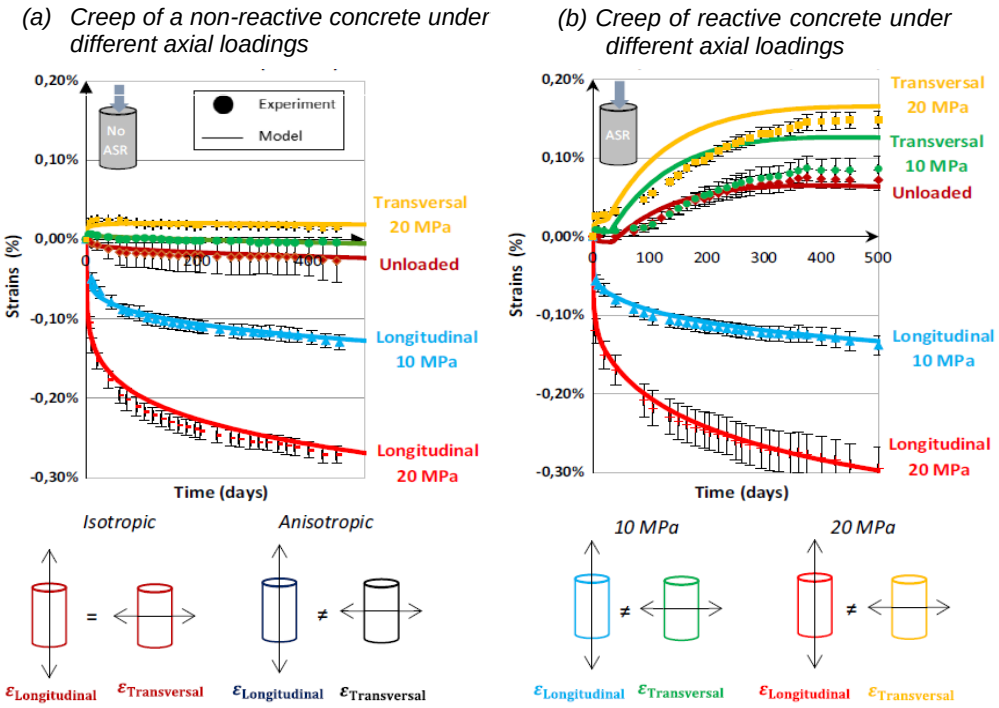

Figure 3.19: Comparison of creep and swelling for non-reactive concrete cylinders (a) and reactive cylinders (b) in free condition or 10MPA and 20MPa of axial compression (Experiments from Multon et al. [60] and modelling from Morenon et al. [52])

Another impact of creep is at microscale, where creep strains of cement paste around swelling zones could absorb a part of swelling without cracking. This phenomena has been proposed by Giorla et al. in [9], however their demonstration was based only on a meso-scopic numerical simulation. One of their conclusions was that only a creep law based on stress criterion would be able to consider this effect, but the simulation was bi-dimensional and their creep law was not fitted on creep tests of cement paste. Whatever the creep law, it is clear this phenomenon exists and should be considered in numerical models.

3.3.3 Interest of poro-mechanical framework to combine swelling, creep and shrinkage

To consider creep, it is possible resorting to a poro-mechanical framework (Figure 3.20 adapted from [63]). The creep model (Kelvin and Maxwell modules in Figure 3.20) is then combined with AAR gel pressure (*Pg* in Figure 3.20).

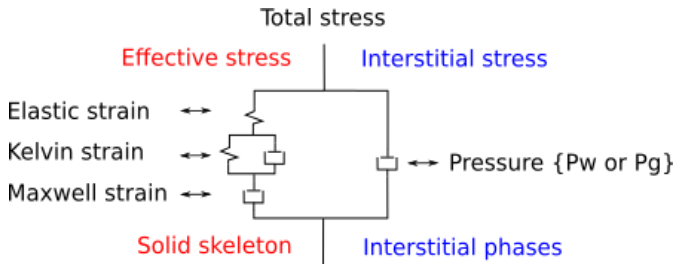

Figure 3.20: Poro-mechanics framework combining the creep model [63] and the gel pressure model (equation 30)

The poro-mechanics formulation combining gel pressure *Pg* and stresses surrounding swelling particles is then given by equation (35) where $\tilde{\sigma}_I'$ is a principal stress in the solid skeleton (left branch in Figure 3.20), P^g the gel pressure and P^w the water pressure (negative in case of drying, leading to

the concrete shrinkage). With this formulation, the concrete swelling is the physical consequence of the gel pressure at micro-scale.

$$\tilde{\sigma}_I = \tilde{\sigma}'_I - b^g P^g - b^w P^w \tag{35}$$

As shown in Figure 3.20 relative to the creep model [63], the total strain is divided into a elastic part, a Kelvin part and a Maxwell part, like in a classic Burger visco-elastic model (left branch in Figure 3.20). The originality of the creep model proposed is its incremental formulation with internal variables, well adapted to non-linear finite elements codes. This model considers the time logarithmic trend of creep [64] through a consolidation function (equation 37), which links the Maxwell characteristic time τ_I in equation (36) to the Maxwell strain ε_I^M through equation (37).

$$\frac{\partial \varepsilon_I^M}{\partial t} = \frac{\varepsilon_I^E}{\tau_I} \tag{36}$$

$$\tau_I = \frac{\tau_{ref}}{k} exp\left(\frac{\varepsilon_I^M}{k\varepsilon_I^E}\right) \tag{37}$$

In equation (37) τ_{ref} and k are fitted constants to quantify, respectively, the creep velocity and potential of concrete. Thank to this method, an anisotropic and incremental implementation of the creep model in finite element codes is facilitated, allowing the combination of creep with the incremental evolution of the gel pressure model. Details of the creep and shrinkage models are given in [63]. Comparisons between Poro-mechanics model's results and Multon's experimental results are plotted in Figure 3.19.

3.3.4 Interest of poro-mechanical framework to discern localized and distributed cracking

The interest of poro-mechanics is that all strains of concrete matrix are taken into account to assess the gel pressure, as formulated in equation (30), and, in return, the gel pressure acts on all strains considered in the model: elastic and creep strains as illustrated in Figure 3.20, but also plastic strains used to model distributed micro-cracking and localized cracking as illustrated in Figure 3.21. In Figure 3.21, it is worth noting that diffuse cracking (located in the left branch of the scheme) is mitigated by tensile creep of solid skeleton, and that opening and reclose of localized cracks (at the top of the scheme) or crushing (at the bottom) are induced by total stress acting at structural scale.

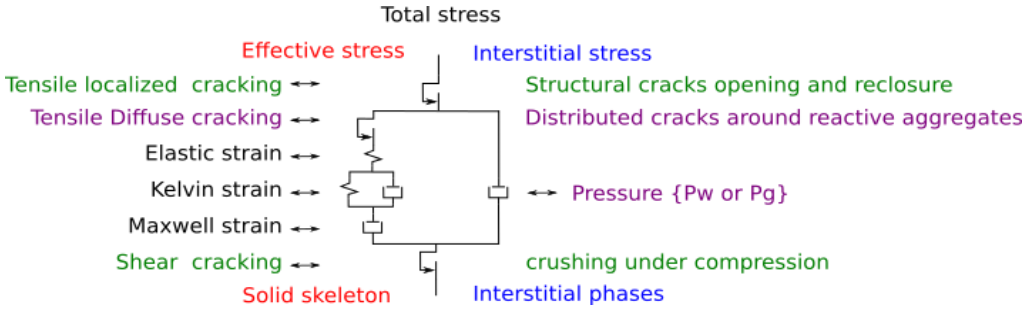

Figure 3.21: Poro-mechanics framework combining the creep model [63] (equation 36) ,the gel pressure model (equation 30), and the plastic strains for structural cracking (in green) and distributed cracking induced by AAR (in purple, and corresponding to equation 34)

The plastic strains corresponding respectively to the localized cracks, to the diffuses cracking induced by AAR, and to the crushing, are stored in separated tensors built by associated plastic flows for the tensile cracks (equation 38 and 39), and a non-associated plastic flow for the crushing (equation 40).

$$\frac{\partial \varepsilon_I^{pt}}{\partial t} = d\lambda_I \frac{\partial f_I^t}{\partial \tilde{\sigma}_I} \tag{38}$$

In (38) f_I^t are the principal stress criteria (or Rankine criteria) defined by equation (39)

$$f_I^t = \tilde{\sigma}_I \ - \tilde{R}t \tag{39}$$

With $\tilde{R}t$ the initial tensile strength of concrete.

$$\frac{\partial \varepsilon_I^{pc}}{\partial t} = d\lambda_c \frac{\partial F^c}{\partial \tilde{\sigma}_I} \tag{40}$$

In (40) F^c is the Drucker Prager yield surface [65] associated to the Drucker Prager criterion (41). In a Drucker Prager yield surface the friction coefficient is replaced by the dilatancy coefficient in order to manage the concrete volume change under crushing in compression, an example of concrete dilatancy in compression is given in Figure 3.23 (b).

$$f^c = \sqrt{\frac{\bar{\bar{\tilde{\sigma}}}^d : \bar{\bar{\tilde{\sigma}}}^d}{2}} - \left(\tilde{R}c\left(\frac{1}{\sqrt{3}} - \frac{\delta}{3}\right) - \delta\frac{tr(\bar{\bar{\tilde{\sigma}}})}{3}\right) \tag{41}$$

In (41) $\bar{\bar{\tilde{\sigma}}}^d$ is the deviatoric part of the stress tensor and $\tilde{R}c$ the compressive strenght of concrete.

3.3.5 Damage induced by swelling reactions

All experiments show a decrease of Young modulus with AAR and DEF swelling. The simplest way to link these two phenomena is a correlation function published by Capra and Sellier in [16]. This correlation was initially fitted on ISE and Larive's tests, but further experiments do not contradict this relationship. The initial form of this law corresponds to equation (42).

$$D_I^{tg} = \frac{\varepsilon_I^{pg}}{\varepsilon^{kg} + \varepsilon_I^{pg}} \tag{42}$$

In (42), ε^{kg} is a fitting parameter equal to 0.3% according to [16]. The evolution of D_I^{tg} is illustrated in Figure 3.22 where the values of $1 - D_I^{tg}$ and $1 - D_I^{cg}$ are compared to ISE experimental results. The damage induced by AAR measured in compression tests was less than in tension. The cause is usually attributed to micro-cracks re-closures during compression tests which provide a partial stiffness recovering; to consider this effect Capra and Sellier proposed equation (43), where exponent α manages the reclosure. It varies theoretically from 0 (none effects of micro cracks on compression's stiffness) to 1 (greater effect in compression than in tension). Their fitting on ISE tests led to $\alpha \approx 0.15$.

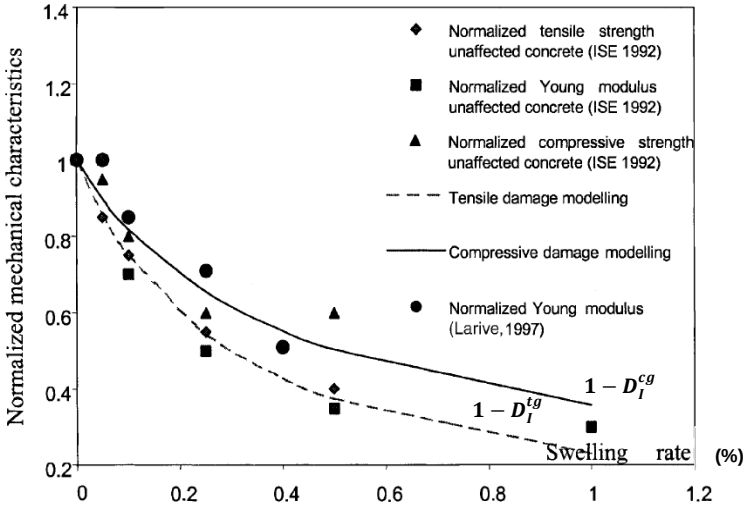

Figure 3.22: Tensile damage D_I^{tg} and compressive damage D_I^{cg} induced by AAR (adapted from [16]).

$$D_I^{cg} = 1 - \left(\left(1 - D_{II}^{tg}\right)\left(1 - D_{III}^{tg}\right)\right)^{\alpha} \tag{43}$$

3.3.6 Coupling between damages due to swelling and other damages

In order to consider both effects of diffuse cracks due to AAR, localized cracks in tension and cracks due to crushing in compression is based on a weakest link formulation initially proposed by Sellier and Bary in [66]. According to this formulation a tensile damage in a given principal direction D_I^t can be induced either by shear D^s , by localized cracks D_I^{tl} , or by AAR D_I^{tg} (cf. Equation 44)

$$1 - D_I^t = (1 - D^s)(1 - D_I^{tl})\left(1 - D_I^{tg}\right) \tag{44}$$

The damage affecting compressive stresses (equation 45) depends on shear damage D^s or on AAR compression damage (equation 43), and on a localized reclosure function $\mathcal{R}_I$ (in equation 46) which allows to manage structural cracks opening and reclose.

$$1 - D_I^c = (1 - D^s)\left(1 - D_I^{cg}\right) \tag{45}$$

Once tensile and compressive anelastic strain assessed solving the equations associated to the scheme of Figure 3.21, the undamaged principal stresses $\tilde{\sigma}_I$ (equation 35) are known. The next step consists to affected them by the damages to obtain the structural stress of the damaged swelling concrete (equations 46). It is worth noting that, as damages are computed in each principal direction of stresses, the behaviour of concrete becomes orthotropic.

$$\begin{aligned} &\sigma_I = (1 - D_I^t)\tilde{\sigma}_I \text{ if } \tilde{\sigma}_I \geq 0 \\ &\sigma_I = (1 - D_I^c)\mathcal{R}_I\ \tilde{\sigma}_I \text{ if } \tilde{\sigma}_I < 0 \end{aligned} \tag{46}$$

Figure 3.23 illustrates the uniaxial behaviour law of a concrete cube 10cm edge, before (in black) and after (in red) an isotropic AAR swelling of 0.3%. In Figure 3.23, compressive cycles are less affected by AAR then tensile cycles; this is the consequence of exponent $\alpha = 0.15$ which, being lesser then 0.5 in equation (43), consider the reclosure of cracks. Indeed, the swelling at 0.3% induces a tensile

strength loss of 50%, while the compressive strength loss is only 18%. The Young modulus becomes then anisotropic and unilateral because it depends for each principal stress on its sign (equations 46).

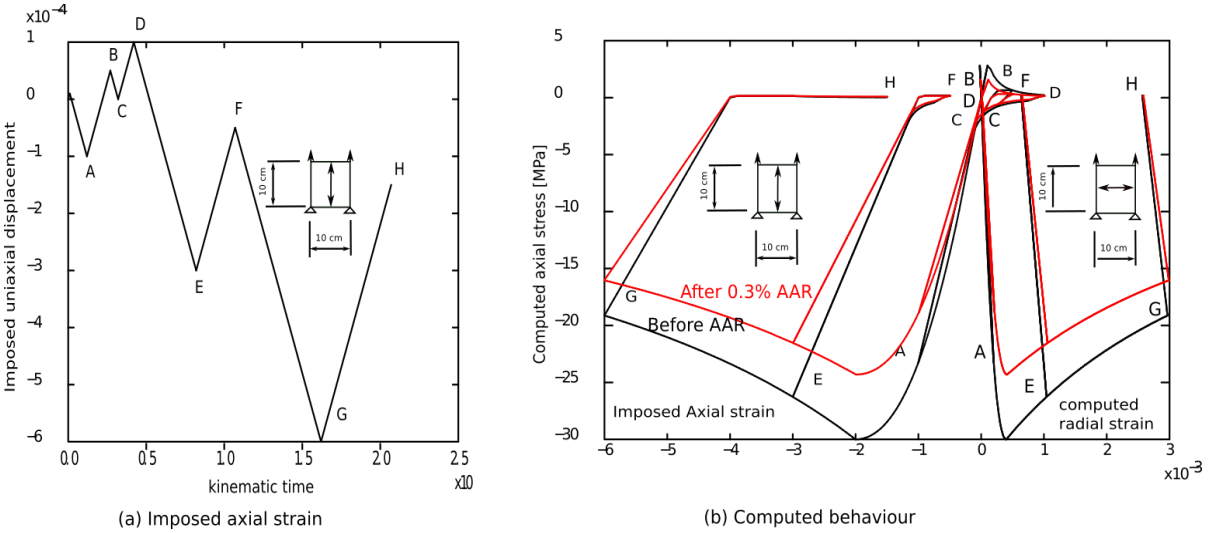

(a) Imposed axial strain (b) Computed behaviour

Figure 3.23: (a) imposed axial strain on a 10cm X 10 cm concrete cube, (b) behaviour law: in black before AAR, in red after 0.3% free swelling, computed with the model developed in LMDC Toulouse [67]. The concrete block characteristics before AAR swelling were *Rc=30MPa, Rt=3MPa, E=30GPA*,

3.3.7 Interactions with reinforcements

According to Goveski et al. in [17], reinforcements reduce significantly swellings; so they propose using an empirical relationship to link the swelling reduction to the reinforcement ratio. Unfortunately, this approach remains a valuable approximation only in case of unloaded structures. Indeed, when the structures are loaded with tension or compression, the prevented effect of the reinforcements towards the swelling of AAR is amplified or reduced, because the stress in the concrete then depends not only on the reinforcement ratio, but also on the interaction between the reinforced concrete and the external loads. This is the reason why it is not sufficient considering reinforcement effects on swelling through an empirical relationship established on unloaded reinforced concrete blocks. A more realistic method is to explicitly mesh reinforcements as in [33], [55], [68], this method is only usable as long as the reinforcement mesh does not weigh too much down the numerical model. For large civil engineering structures, meshing all the reinforcement is sometimes difficult and another solution must be used. This is the main reason why Goveski et al. in [17] resorted to a modified swelling law. The method we adopt in [68][69] to combine reinforcement and concrete in larges reinforced structures consists simply combining the poromechanics model presented above with a distributed reinforcements model which allows avoiding meshing the reinforcements; the resulting behaviour law corresponds to homogenized material in which reinforcements and concrete are combined in a parallel scheme for each principal direction of stress as schemed in Figure 3.24, and expressed by equation (47).

$$\sigma = \left(1 - \sum_{r=1}^{n} \rho_r\right) \overline{\overline{\sigma}}^c + \sum_{r=1}^{n} \rho_r \, \sigma_r \, \overrightarrow{e_r} \otimes \overrightarrow{e_r} \qquad (47)$$

In equation (47) $\overline{\overline{\boldsymbol{\sigma}}}^c$ (in the left branch) is the stress tensor in the swelling concrete, corresponding to the poromechanics model schemed given in Figure 3.21, ρ_r the reinforcement's densities oriented in the direction $\overrightarrow{e_r}$, σ_r the stress in the reinforcement number r. Each reinforcement can be either a pre-stressing wire or a passive rebar as illustrated in Figure 3.24. This method allows also considering the sliding between reinforcements and concrete without meshing the reinforcements. The principle consists of using a Helmholtz formulation which links the total strain of homogenized material ε to the reinforcement elastic strain (ε^{re} *in* equation 48). Details concerning this aspect are published in [71].

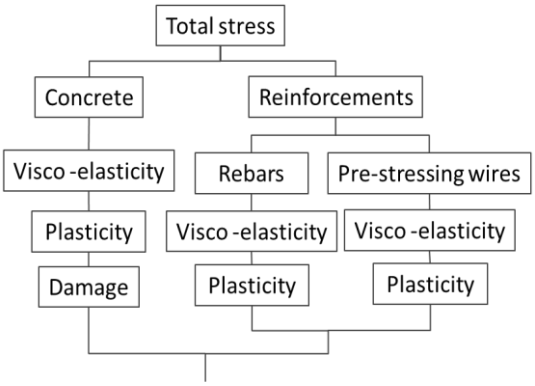

Figure 3.24: Combination of concrete and reinforcements to obtain a homogenized reinforced concrete material (schemed inspired from [70])

$$\varepsilon^{re} - \frac{E^r D^r}{4H^i}\frac{\partial^2 \varepsilon^{re}}{\partial x^2} = \varepsilon - \varepsilon^{rp} - \varepsilon^{rv} \quad (48)$$

In equation 48, x is the reinforcement local axes, E^r is the Young's modulus of the reinforcement, Hi the secant modulus of the concrete/reinforcement interface behaviour law, D^r the equivalent diameter of the rebar, ε^{re} its elastic strain, ε^{rp} its plastic strain, ε^{rv} its viscous strain (causing relaxation), and ε the mechanical strain of the reinforced concrete. Thank to this equation, the sliding of pre-stressed wire and passive reinforcements can be treated numerically without meshing them as illustrated in [70].

4. FITTING METHODOLOGY AND MODELLING QUALITY INDICATORS

4.1 Fitting methodology

As illustrated in Figure 4.1, for numerous structures affected by AAR and DEF, only a part of the swelling chronology is known, because measurements instruments like pendulums, invar rods, altimetry landmarks, vibrating wires, flat cylinders or optical fibres are often installed after that the first cracking are visible and not just after the structure building. Using only this time domain to fit a model can lead to wide misestimating of final swelling. This is due to the fact that all models are based on two main parameters: the kinetic of the chemical reaction (τ_{ref} in equation 7 and 8) and the swelling potential $\varphi^{g\infty}$ in equation (21 or 30), and these two parameters can balance one-another as illustrated in the summarizing correlation (49).

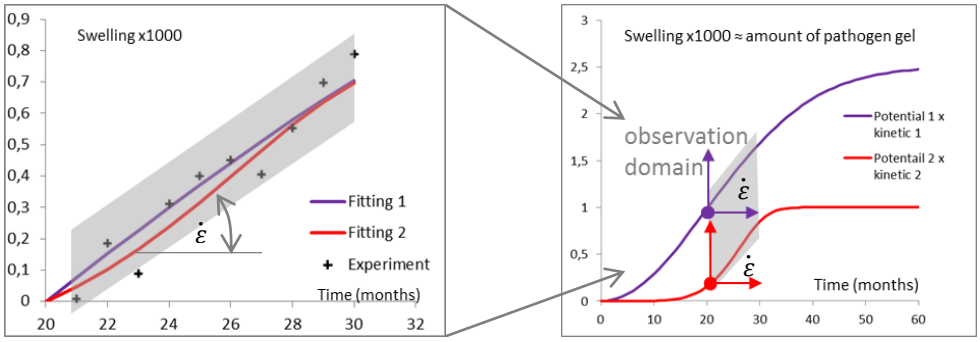

(a) Observed swelling in a limited time domain

(b) Two admissible solutions fitting a model only on swelling kinetic

Figure 4.1: Different fitting possibilities using only measured displacements in the field induced by swelling (fitting 1 could overestimate final swelling while fitting 2 underestimate it)

$$\dot{\varepsilon} \sim \dot{A}(\tau_{ref}^{g}).\,\varphi^{g\infty} \tag{49}$$

To limit, or avoid, an arbitrary fitting of kinetic and swelling potential, several methods inventoried in [72] can be combined. Among these methods, the one proposed by LMDC Toulouse consists in performing chemical and physical tests on aggregates to measure the advancement of the reaction in one hand, and in the other hand using some displacements of the affected structure to fit the swelling potential. Even if this method is relatively complex to perform, it allows splitting clearly the fitting of the kinetic and the fitting of the swelling potential. The first application of this fitting methodology was published by Grimal et al. in [73] and by Sellier et al. in [10]. The principle consists in two main stages: fitting first of chemical kinetic (parameter τ_{ref}^{g}) of the reaction with laboratory's tests, and once τ_{ref}^{g} known, adapt the swelling potential $\varphi^{g\infty}$ in the field.

4.1.1 Fitting of the chemical kinetic

First, the aggregates of drilled specimens are extracted and their residual swelling potential are measured in standard conditions. As specimens are chosen in different zones of the structure, the advancement of the reactions differs from a drilling zone to another; specifically, the dry zones are not affected by the swelling reaction while wet zones present the maximal swellings in the field. By comparison of residual swelling of these two zones the advancement of the reaction in the field can be determinate. More the residual swelling during the test, less the advancement in the field as illustrated in Figure 4.2.

(a) Core samples→ (b) Hydrochloric acid attack (1M) → (c)Recovered Aggregate (after sifting)

(d) Mortar bars made with crushed aggregates extracted

(e) Exploitation of differential swellings of mortars to assess chemical advancement A(t) (cf. equation 50)

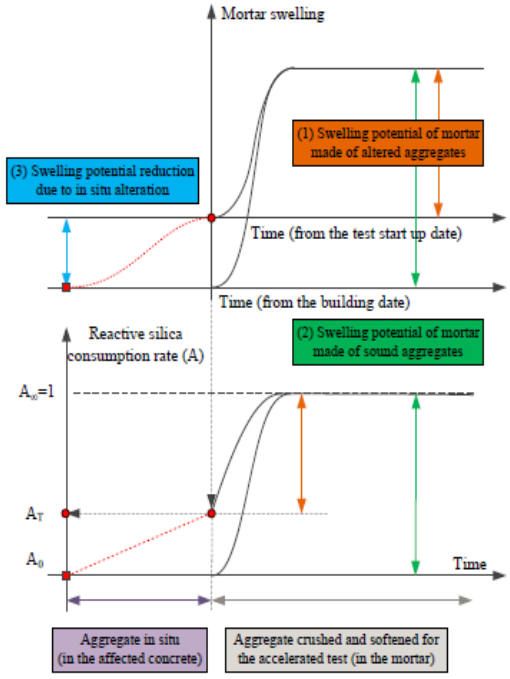

Figure 4.2: Principle of the methodology proposed in LMDC Toulouse with EDF-CIH to quantify the advancement A(t) of a swelling reaction: from (a) specimen drilled in the structure, until (e) assessment of the advancement of the reaction in the field deduced from differential swellings of mortar bars made with crushed aggregates extracted from concrete

Once the advancement assessed, the past of the drilled specimen is considered, with the past real temperature T(t) in the field, and the past real water saturation rate Sr(t). If these two variables are assumed quasi constant during the past of the structure, the characteristic time τ_{ref}^{g} of the reaction, used in equation (8) is given by equation 50. Otherwise, if the variations of T and Sr are not negligible, $\dot{A}$ must be numerically integrated considering the evolutions of T and Sr in the field since the building date, and τ_{ref}^{g}results from a minimization of the error A(t).

$$\tau_{ref}^{g} = \frac{-t}{ln(Sr - A(t))}\left(\frac{Sr - S_r^{th}}{1 - S_r^{th}}\right)^2 \qquad (50)$$

This method can be used either on the entire aggregate distribution, or after sieving, on different sizes ranges of aggregates. In this last case, a kinetic can be associated to each size of aggregate as explained in [15]. In equation (50) t is the age of the structure (since the construction), Sr is the saturation rate of the drilled specimen in the field, $A(t)$ is the advancement deduced from residual swelling tests in standard conditions, S_r^{th} the threshold saturation rate under which the reaction stops (cf. equation 8).

4.1.2 Fitting of the swelling potential

Once the kinetic of the chemical reaction known (provided by the characteristic time τ_{ref}^{g} , by equation 50), the swelling potential of concrete is determinate by finite element inverse analysis. The aim of this stage is to find the swelling potential ($\varphi^{g\infty}$ used in equation 30), which is a scalar parameter, to retrieve the displacements' trends for some instrumented points of the structure in the field. This stage starts with the modelling of saturation field as illustrated in Figure 4.3.

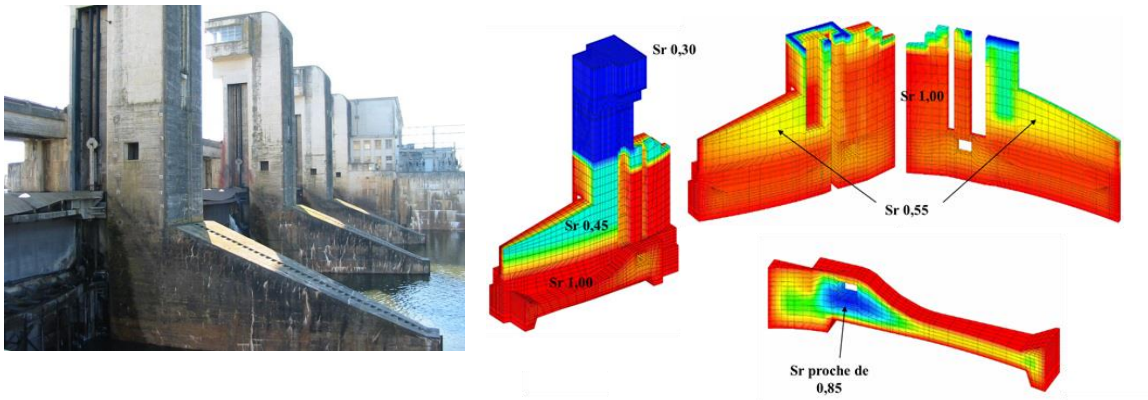

Figure 4.3: Water saturation rate (Sr) field computed with in situ boundary conditions, and saturation rates of drilled specimens collected at different locations of a dam [74].

The saturation rate chronology and the temperature chronology allow to compute the displacements of the structure, which can be compared with the measured ones. As mentioned above, the displacements in the fields are usually not known since the construction date, so, only the trend of swelling are compared for some chosen points. The swelling potential is then fitted to minimize the difference of swelling rates computed and measured as illustrated in Figure 4.4.

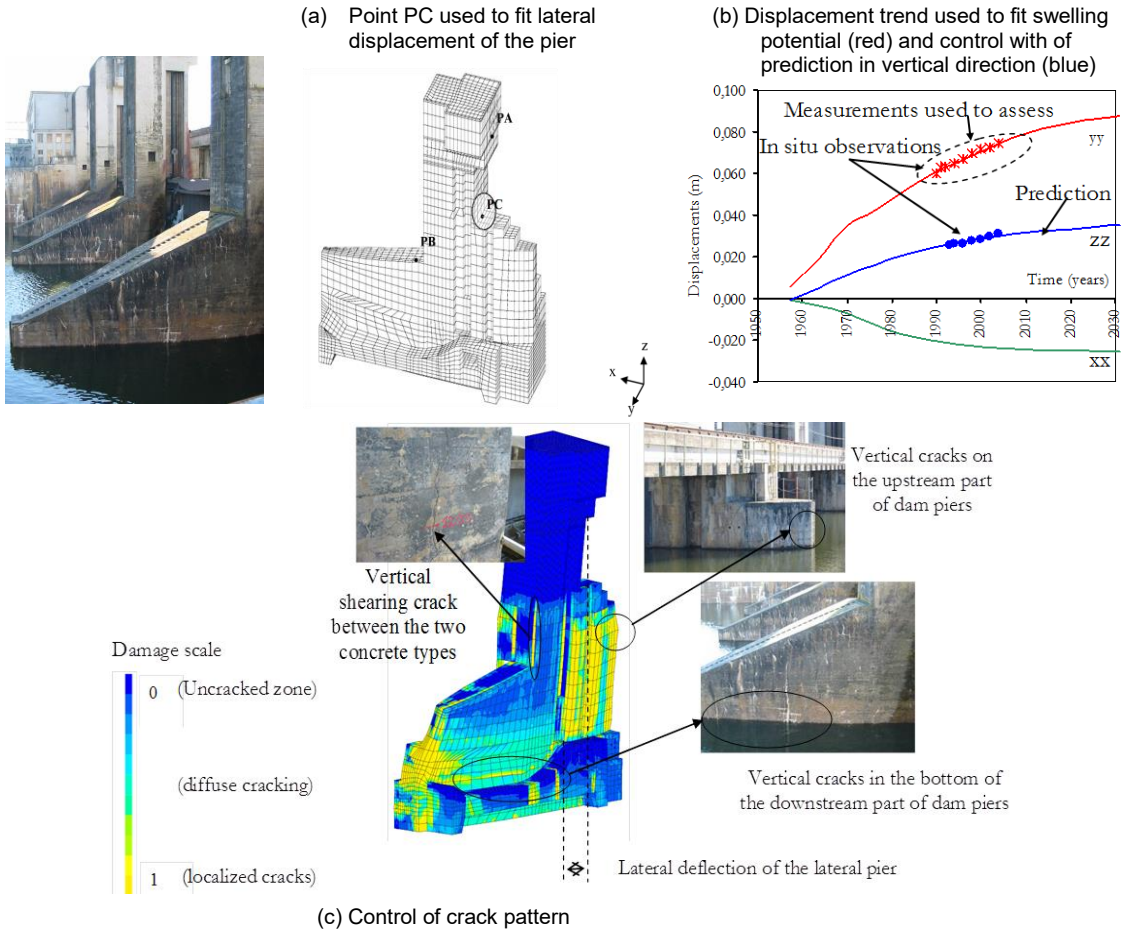

Figure 4.4: Fitting of swelling potential ($\varphi^{g\infty}$ in equation 30) by inverse analysis of the displacement of point C in horizontal direction; control of the model by comparison of displacements in the vertical direction and control of the conformity of the predicted cracking pattern to the observed one (reinforced concrete pier of a dam gate [15]).

4.2 Quality indicators and using of the model

As illustrated in Figure 4.4, the conformity to the displacements of different instrumented points of the structure on the one hand, and the obtaining of a realistic crack pattern on the other hand, are the two main guarantees of a correct fit of the model. Once this step is completed, the prediction of structural behaviour can be made for the following decades. Such simulations are now currently performed, for instance by Grimal et al. at EDF-CIH in order to quantify the benefits effects of steel tie rods used to strength the piers of dam-gates [74] (Figure 4.5), or to assess the benefits and limits of slot's sawings of gravity-dams (Figure 3.18).

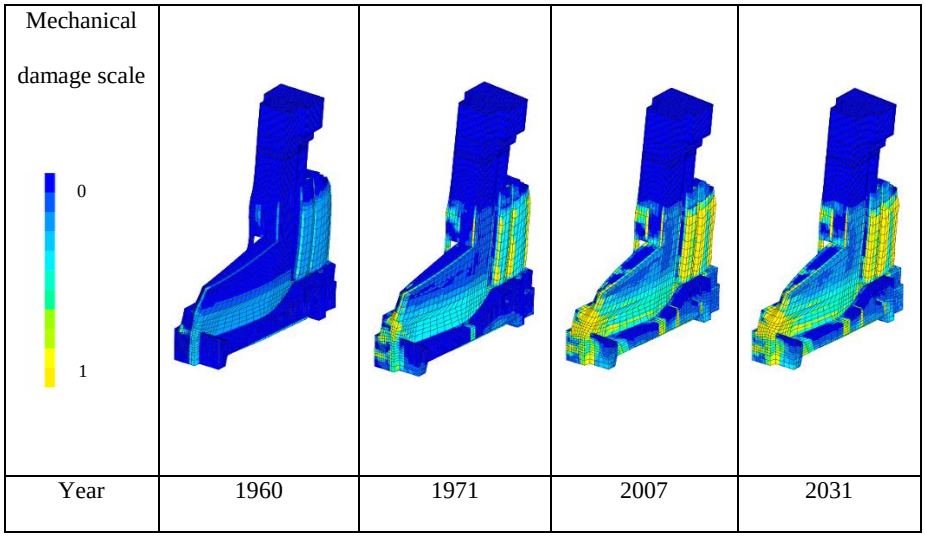

Figure 4.5: predicted behaviour and tilting of a pier of a gate dam (from Grimal et al. [15]).

A same methodology was applied by Morenon et al. to dams affected by DEF and by Vo et al. to a nuclear confinement vessel. Results and details of the methodology adapted to the DEF are available in [75], [76].

5. CONCLUSION

Modelling structures affected by AAR or DEF starts with the understanding of chemical reactions at nanoscale. At this scale the mineralogy of aggregates, their sizes, the composition of the cement paste and the thermohydric past of the structure play a major role, resulting in a more or less fast chemical reaction. The state variables chosen to consider these phenomena are relatively limited for AAR, since an appropriate definition of the reaction advancement A(t) can be done with only one variable (either the alkali consumption or the reactive silica consumption), but as mentioned in 3.1.1 further enhancement could be done to have a better assessment of the AAR product fluidity. On the other hand, it is more difficult to simplify the different phenomena underlying DEF. In fact, DEF occurs if concrete is subjected to a temperature rising which causes the dissolution of primary ettringite, but if the temperature is maintained a too long time, aluminates can be taken definitively by C-S-H to form Hydrogarnet and secondary ettringite does not occur by default of aluminates. This phenomenon explains why a pessimum in terms of heat duration exists for DEF. To consider this effect it is necessary to compute the past evolutions of sulphates, aluminates and alkali in concrete, their concentrations are the state variables of DEF chemical models, together with the ettringite and other aluminates hydrates. As chemical reactions kinetics are sensitive to temperature, the temperature field is needed for each date of mechanical calculus. Another important state variable is the water saturation rate, which controls the ions mobilities and then the kinetic of the reactions. Like for the temperature, the water saturation rate must be available for each step of mechanical simulation. Concerning the mechanical behaviour of concrete affected by swelling reactions, only an analysis of phenomena occurring at meso-scale (the scale of aggregates and gel spots) allows understanding the swelling mechanism. The linear micro-mechanics analysis provided in chapter 3.2.2.2 of this paper supplies the main relationships explaining the anisotropy of swelling; this is a problem of micro-crack initiation at the aggregate - cement paste interface, where the maximal orthoradial stresses concentrations induced by aggregate's swelling occur. If these stresses concentrations are balanced by the ones coming from external compressive loading, the crack propagations are impeded in the plane orthogonal to the external compression, and swelling becomes anisotropic. These considerations explain both the swelling anisotropy and the dependence of swelling on compressive loadings. To move from the meso scale to the structural scale, it is convenient to resort to a poro-mechanical formulation in which plastic deformations depend on plastic criteria deduced from meso-scale considerations. This formulation, more physic than previous empirical laws used by engineers to reduce swelling in compressed directions, is more efficient to simulate multi axial loaded concretes

without too many fitted parameters. More, it allows to combining relatively easily the phenomenon of creep with the effect of AAR gel of DEF pressure, and as illustrated in 3.3.3, the creep amplitude and the swelling amplitude of AAR are of the same order. The poromechanics formulation can be combined with reinforcements models to treat the case of large reinforced concrete structures, this combination must be done without changing the mechanical behaviour law, but considering concrete and reinforcements in parallel (cf. chapter 3.3.7). Once all these phenomena considered, a clear fitting methodology must be defined in order to avoid a misestimating of swelling potential. The methodology detailed herein consists to assess, firstly the kinetic of the reaction using mainly tests laboratory performed on material retrieved in the field, and secondly the swelling potential by inverse analysis of displacements measured on the real structure (cf. chapter 4.1). A control of calibration process can be done using displacements of points never used for fitting, and comparing the predicted and the observed crack patterns. Once controlled, the numerical model can be used to predict efficiency of repair methods like steel tie rods or slot cuttings.

Researches currently performed in LMDC Toulouse on this topic consist in one hand to clarify the reinforced concrete behaviour law usable for very large reinforced concrete structures like nuclear confinement vessels and large dams [68][69], and in the other hand to propose a behaviour law for structural finite element modelling in which the micro-mechanical aspects described in chapter 3.2.2.2 will be fully integrated through analytical methods in the structural behaviour law [62]. The main problem to solve in the context of reinforced structure is the modelling of partial irreversibility of the gel migration between AAR spots and micro-cracks. Concerning the link between meso and structural models, the main problem consists to improve the homogenization schemes to consider simultaneously elastic and an-elastic strains fields, in order to have a full coupling between the swelling, the creep [62], the micro-cracks opening and reclosing, and the migration of chemical reaction products between reactive spots and porosity or cracks.

6. ACKNOWLEDGEMENTS

All the methods and softwares used to illustrate this document would not exist without many internal and external collaborations. Among the main companies and institutions involved in the development of the models are EDF-CIH with MM. E. Bourdarot, E. Grimal, P. Kolmayer and C. Bodel, EDF Septen with M. B. Masson, ANDRA with M. X. Bourbon, VINCI construction grands projets with MM. L. Boutillon and L. Linger, C. Noret and P. Antiniac of Engie Tractable, M. A. Millard of CEA. May they find here the expression of my gratitude for the trust granted and the means allocated.

The PhD students involved and supervised were mainly S.Poyet, E.Grimal, M.Salgues, P. Morenon and D. Vo with EDF, Y.Thiebault with VINCI, W Ladaoui, H.Cagnon and F. Manzoni with Andra, C.Lacombe with Engie. Thank you to them for their sympathy and for the work done.

S. Feldman of NIST is also thanked for his kind provision of SEM photos. My dear colleagues and friends with whom fruitful discussions are always a pleasure: Mm M. Morenville-Regourd, MM. B.Capra and B.Bary, (during the period at ENS Cachan and the University of Paris Est), S. Multon, T. Vidal, L. Lacarrière, and A.Papon (during the period at the LMDC, at the University of Toulouse).

Mr. F.Toutlemonde, R.P Martin, B.Nedjar, of IFSTTAR Paris; Pr V. Saouma of Boulder University; Pr B.Fournier and P.Sanchez of the universities of Quebec, M. A. Leeman of EMPA, and many other colleagues met at the ICAAR or DSC conferences, and in the EOCD-NEA or RILEM technical committees, are also warmly thanked for their constructive discussions.

7. REFERENCES

[1] R. G. Charlwood, S. V. Solymar, and D. D. Curtis, “A review of alkali aggregate reactions in hydroelectric plants and dams,” 1992.

[2] S. Multon and F. Barin, “Estimation of the Residual Expansion of Concrete Affected by Alkali Silica Reaction,” *J. Mater. …*, no. January, pp. 54–62, 2008, Accessed: Feb. 17, 2013. [Online]. Available: http://ascelibrary.org/doi/abs/10.1061/(ASCE)0899-1561(2008)20:1(54).

[3] V. Saouma and L. Perotti, “Constitutive model for alkali-aggregate reactions,” *ACI Mater. J.*, vol. 103, no. 3, p. 194, 2006, Accessed: Jan. 28, 2012. [Online]. Available: http://civil.colorado.edu/~saouma/AAR/Saouma-AAR-1.pdf.

[4] J. Liaudat, I. Carol, C. M. López, and V. E. Saouma, “ASR expansions in concrete under triaxial confinement,” *Cem. Concr. Compos.*, vol. 86, pp. 160–170, Feb. 2018, doi: 10.1016/j.cemconcomp.2017.10.010.

[5] R.-P. Martin, D. Siegert, and F. Toutlemonde, “Experimental analysis of concrete structures affected by DEF: Influence of moisture and restraint,” in *Thermo-hydromechanical and chemical coupling in geomaterials and applications*, 2008, pp. 334–340.

[6] Z. Shi, A. Leemann, D. Rentsch, and B. Lothenbach, “Synthesis of alkali-silica reaction product structurally identical to that formed in field concrete,” *Mater. Des.*, vol. 190, p. 108562, May 2020, doi: 10.1016/j.matdes.2020.108562.

[7] V. Saouma, *Diagnosis & Prognosis of AAR Affected Structures*, Springler., vol. 31. Cham: Springer International Publishing, 2021.

[8] O. Mielich, H. Özkan, and H. W. Reinhardt, “Creep Behaviour of Alkali-Silica Reaction Damaged Concrete With Slow-Reacting Aggregates,” 2017.

[9] A. B. Giorla, K. L. Scrivener, and C. F. Dunant, “Influence of visco-elasticity on the stress development induced by alkali–silica reaction,” *Cem. Concr. Res.*, vol. 70, pp. 1–8, Apr. 2015, doi: 10.1016/J.CEMCONRES.2014.09.006.

[10] A. Sellier, E. Bourdarot, E. Grimal, S. Multon, and M. Cyr, “Structural monitoring and residual reactive silica measurement combination for finite element analysis of structure affected by ASR,” in *ACI Journal proceedings*, 2009, pp. 1–30.

[11] P. Morenon, S. Multon, A. Sellier, E. Grimal, F. Hamon, and P. Kolmayer, “Flexural performance of reinforced concrete beams damaged by Alkali-Silica Reaction,” *Cem. Concr. Compos.*, vol. 104, 2019, doi: 10.1016/j.cemconcomp.2019.103412.

[12] D. Vo *et al.*, “Homogenized reinforced concrete model for the evaluation of ASR affected structures Abstract,” in *FIB PhD Symposium 2021*, no. 1.

[13] Y. Kawabata, J.-F. Seignol, R.-P. Martin, and F. Toutlemonde, “Macroscopic chemo-mechanical modeling of alkali-silica reaction of concrete under stresses,” *Constr. Build. Mater.*, vol. 137, pp. 234–245, Apr. 2017, doi: 10.1016/J.CONBUILDMAT.2017.01.090.

[14] M. Shakoorioskooie, M. Griffa, A. Leemann, R. Zboray, and P. Lura, “Alkali-silica reaction products and cracks: X-ray micro-tomography-based analysis of their spatial-temporal evolution at a mesoscale,” *Cem. Concr. Res.*, vol. 150, p. 106593, Dec. 2021, doi: 10.1016/J.CEMCONRES.2021.106593.

[15] A. Sellier, E. Bourdarot, S. Multon, M. Cyr, and E. Grimal, “Combination of structural monitoring and laboratory tests for the assessment of AAR-swelling: application to a gate structure dam,” *ACI Mater. J.*, vol. 106, no. 3, pp. 281–290, 2009.

[16] B. Capra and A. Sellier, “Orthotropic modelling of alkali-aggregate reaction in concrete structures : numerical simulations,” *Mech. Mater.*, vol. 6, no. December, 2002.

[17] A. Sellier, E. Grimal, S. Multon, and E. Bourdarot, *Swelling Concrete in Dams and Hydraulic Structures: DSC 2017*. Chambéry: ISTE Wiley, 2017.

[18] CIGB and ICOLD, “International Commission on Large Dams.” https://www.icold-cigb.org/ (accessed Feb. 17, 2020).

[19] S. Poyet *et al.*, “Influence of water on alkali-silica reaction: Experimental study and numerical simulations,” *J. Mater. Civ. Eng.*, vol. 18, no. July/August, p. 588, 2006, Accessed: Jan. 28, 2012. [Online]. Available: http://link.aip.org/link/?JMCEE7/18/588/1.

[20] C. Larive, “Compte rendu de la XI Conférence internationale sur les réactions alcalis-granulats dans le béton,” 2001, pp. 89–94.

[21] S. Multon and F. Toutlemonde, “Water distribution in concrete beams,” *Mater. Struct.*, vol. 37, no. July, pp. 378–386, 2004, Accessed: Feb. 17, 2013. [Online]. Available: http://www.springerlink.com/index/8Q5K7U6378134864.pdf.

[22] E. Grimal, A. Sellier, Y. Le Pape, and E. Bourdarot, “Creep, Shrinkage, and Anisotropic Damage in Alkali-Aggregate Reaction Swelling Mechanism-Part II: Identification of Model Parameters and Application,” *ACI Mater. J.*, vol. 105 No 3, pp. 236–242, 2008, doi: 10.14359/19819.

[23] B. Capra and A. Sellier, “Orthotropic modelling of alkali-aggregate reaction in concrete structures: Numerical simulations,” *Mech. Mater.*, vol. 35, pp. 817–830, 2003, doi: 10.1016/S0167-6636(02)00209-0.

[24] N. W. Hayes, A. B. Giorla, W. Trent, D. Cong, Y. Le Pape, and Z. J. Ma, “Effect of alkali-silica reaction on the fracture properties of confined concrete,” *Constr. Build. Mater.*, vol. 238, p. 117641, Mar. 2020, doi: 10.1016/J.CONBUILDMAT.2019.117641.

[25] A. Sellier, E. Bourdarot, E. Grimal, S. Multon, and M. Cyr, “Structural monitoring and residual reactive silica measurement combination for finite element analysis of structures affected by ASR,” in *American Concrete Institute, ACI Special Publication*, 2009, no. 266 SP.

[26] H. Group, “Thermodynamic and mathematical concepts of CHESS J . van der Lee,” *Program*, no. March, 2009.

[27] S. Diamond, R. S. Barneyback, and S. Jr, “On the physics and chemistry of alkali-silica reactions Conference on alkali-aggregate reaction in concrete Cape Town - South Africa , March 30- April 3, 1981.,” 1981.

[28] A. Sellier and B. Capra, “Modélisation physico-chimique de la réaction alcali-granulat: apport au calcul des structures dégradées,” *Rev. Française Génie Civ.*, vol. 1, no. 3, pp. 445–481, Jan. 1997, doi: 10.1080/12795119.1997.9692135.

[29] F.-J. Ulm, O. Coussy, L. Kefei, and C. Larive, “Thermo-Chemo-Mechanics of ASR Expansion in Concrete Structures,” *J. Eng. Mech.*, vol. 126, no. 3, pp. 233–242, Mar. 2000, doi: 10.1061/(ASCE)0733-9399(2000)126:3(233).

[30] C. Larive, “Apports combinés de l’expérimentation et de la modélisation à la compréhension de l’alcali-réaction et de ses effets mécaniques,” Jun. 1997, Accessed: Feb. 19, 2020. [Online]. Available: https://pastel.archives-ouvertes.fr/tel-00520676v1.

[31] V. E. Saouma, R. a. Martin, M. a. Hariri-Ardebili, and T. Katayama, “A mathematical model for the kinetics of the alkali–silica chemical reaction,” *Cem. Concr. Res.*, vol. 68, pp. 184–195, Feb. 2015, doi: 10.1016/j.cemconres.2014.10.021.

[32] E. Grimal, A. Sellier, S. Multon, and E. Bourdarot, “Modeling of structures affected by alkali aggregate reaction,” in *American Concrete Institute, ACI Special Publication*, 2009, no. 266 SP.

[33] P. Morenon, S. Multon, A. Sellier, E. Grimal, F. Hamon, and P. Kolmayer, “Flexural performance of reinforced concrete beams damaged by Alkali-Silica Reaction,” *Cem. Concr. Compos.*, vol. 104, p. 103412, Nov. 2019, doi: 10.1016/J.CEMCONCOMP.2019.103412.

[34] D. Damidot and F. P. Glasser, “Thermodynamic investigation of the CaO Al2O3 CaSO4 H2O system at 50°C and 85°C,” *Cem. Concr. Res.*, vol. 22, no. 6, pp. 1179–1191, 1992, doi: 10.1016/0008-8846(92)90047-Y.

[35] G. Scherer, “Crystallization in pores,” *Cem. Concr. Res.*, vol. 29, no. December 1998, pp. 1347–1358, 1999, Accessed: Feb. 17, 2013. [Online]. Available: http://www.sciencedirect.com/science/article/pii/S0008884699000022.

[36] B. Godart and L. Divet, “The new french recommendations to prevent disorders due to delayed ettringite formation,” HAL CCSD, 2008. Accessed: Jan. 13, 2018. [Online]. Available: https://core.ac.uk/display/50169234.

[37] D. Damidot and F. P. Glasser, “Thermodynamic investigation of the CaO-Al2O3-CaSO4-H2O system at 50°C and 85°C,” *Cem. Concr. Res.*, vol. 22, no. 6, pp. 1179–1191, Nov. 1992, doi: 10.1016/0008-8846(92)90047-Y.

[38] N. Baghdadi, J. Seignol, R. Martin, and F. Toutlemonde, “Effect of early age thermal history on the expansion due to delayed ettringite formation : experimental study and model calibration,” pp. 1–6.

[39] M. Salgues, A. Sellier, S. Multon, E. Bourdarot, and E. Grimal, “DEF modelling based on thermodynamic equilibria and ionic transfers for structural analysis,” *Eur. J. Environ. Civ. Eng.*, pp. 1–26, 2014, doi: 10.1080/19648189.2013.872579.

[40] E. L’Hôpital, B. Lothenbach, G. Le Saout, D. Kulik, and K. Scrivener, “Incorporation of aluminium in calcium-silicate-hydrates,” *Cem. Concr. Res.*, vol. 75, pp. 91–103, Sep. 2015, doi: 10.1016/j.cemconres.2015.04.007.

[41] A. Sellier and S. Multon, “Chemical modelling of Delayed Ettringite Formation for assessment of affected concrete structures,” *Cem. Concr. Res.*, vol. 108, pp. 72–86, Jun. 2018, doi: 10.1016/j.cemconres.2018.03.006.

[42] X. Brunetaud, R. Linder, L. Divet, D. Duragrin, and D. Damidot, “Effect of curing conditions and concrete mix design on the expansion generated by delayed ettringite formation,” *Mater. Struct.*, vol. 40, no. 6, pp. 567–578, Feb. 2007, doi: 10.1617/s11527-006-9163-3.

[43] X. Brunetaud, “Etude de l’influence de différents paramètres et de leurs interactions sur la cinétique et l’amplitude de la réaction sulfatique interne au béton.,” Paris Est, 2005.

[44] C. Famy, K. . Scrivener, A. Atkinson, and A. . Brough, “Influence of the storage conditions on the dimensional changes of heat-cured mortars,” *Cem. Concr. Res.*, vol. 31, no. 5, pp. 795–803, May 2001, doi: 10.1016/S0008-8846(01)00480-X.

[45] M. Al Shamaa, S. Lavaud, L. Divet, G. Nahas, and J. M. Torrenti, “Influence of relative humidity on delayed ettringite formation,” *Cem. Concr. Compos.*, vol. 58, pp. 14–22, 2015, doi: 10.1016/j.cemconcomp.2014.12.013.

[46] S. Poyet *et al.*, “Chemical modelling of Alkali Silica reaction: Influence of the reactive aggregate size distribution,” *Mater. Struct.*, vol. 40, no. 2, pp. 229–239, Jan. 2007, doi: 10.1617/s11527-006-9139-3.

[47] S. Multon and A. Sellier, “Multi-scale analysis of alkali – silica reaction (ASR): Impact of alkali leaching on scale effects affecting expansion tests,” *Cem. Concr. Res.*, vol. 81, pp. 122–133, 2016, doi: 10.1016/j.cemconres.2015.12.007.

[48] J. Liaudat, M. Rodriguez, C. Lopez, and I. Carol, “Recent Developments in Durability Mesomechanics of Concrete, Including Cracking via Interface Elements,” in *Mechanics and Physics of Creep, Shrinkage, and Durability of Concrete*, American Society of Civil Engineers, 2013, pp. 174–181.

[49] A. Sellier, T. Vidal, J. Verdier, and R. Bucher, “Un nouveau critère de fissuration pour les matériaux hétérogènes soumis à des sollicitations multi-physiques,” *Acad. J. Civ. Eng.*, vol. 36, no. 1, pp. 108–111, 2018, doi: 10.26168/AJCE.36.1.27.

[50] T. Mori and K. Tanaka, “Average stress in matrix and average elastic energy of materials with misfitting inclusions,” *Acta Metall.*, vol. 21, no. 5, pp. 571–574, May 1973, doi: 10.1016/0001-6160(73)90064-3.

[51] E. Grimal, A. Sellier, Y. L. Pape, and E. Bourdarot, “Creep, shrinkage, and anisotropic damage in alkali-aggregate reaction swelling Mechanism-Part I: A constitutive model,” *ACI Mater. J.*, vol. 105, no. 3, 2008.

[52] P. Morenon, S. Multon, A. Sellier, E. Grimal, F. Hamon, and E. Bourdarot, “Impact of stresses and restraints on ASR expansion,” *Constr. Build. Mater.*, vol. 140, pp. 58–74, 2017, doi: 10.1016/j.conbuildmat.2017.02.067.

[53] E. Grimal, A. Sellier, Y. L. Pape, and E. Bourdarot, “Creep, shrinkage, and anisotropic damage in alkali-aggregate reaction swelling Mechanism-Part II: Identification of model parameters and application,” *ACI Mater. J.*, vol. 105, no. 3, 2008.

[54] P. Morenon, S. Multon, A. Sellier, E. Grimal, and F. Hamon, “Impact of multi-axial stresses on ASR expansion,” in *15th ICAAR International conference on alkali aggregate reaction in concrete*, 2016, p. 142.

[55] P. Morenon, S. Multon, and A. Sellier, “ASR expansions modelling under multi-axial stresses,” in *16th international conference on alkali aggregate reaction in concrete, lisboa, 16-18 june 2020*, 2020, pp. 1–12.

[56] E. Grimal and S. Multon, “Combination of structural monitoring, laboratory tests and modeling to manage dams degraded by swelling phenomena, application to the dam of Chambon,” in *15th ICAAR International conference on alkali aggregate reaction in concrete*, 2016, p. 33.

[57] O. Coussy, *Poromechanics*. Wiley, 2004.

[58] V. Saouma and L. Perotti, “Constitutive Model for Alkali-Aggregate Reactions,” *ACI Mater. Journal-American Concr. Inst.*, no. 103, 2007.

[59] J. Seignol and V. Le, “Integration of anisotropy , contact elements and creep in RGIB-modulus of the F . E . program ‘ CESAR-LCPC ’: Application to structures affected by internal swelling reactions,” *Concrete*, no. 1985, 2009.

[60] S. Multon, “Evaluation expérimentale et théorique des effets mécaniques de l’alcali-réaction sur des structures modèles,” Université de Marne la Vallée, 2003.

[61] Y. Thiebaut *et al.*, “Effects of stress on concrete expansion due to delayed ettringite formation,” *Constr. Build. Mater.*, vol. 183, pp. 626–641, Sep. 2018, doi: 10.1016/J.CONBUILDMAT.2018.06.172.

[62] C. Lacombe, A. Sellier, T. Vidal, C. Noret, and P. Anthiniac, “Mitigation of AAR structural effects by creep of concrete : experiments and modelling,” in *16th international conference on alkali aggregate reaction in concrete, lisboa, 16-18 june 2020*, 2020, pp. 1–10.

[63] A. Sellier, S. Multon, L. Buffo-lacarrière, T. Vidal, X. Bourbon, and G. Camps, “Concrete creep modelling for structural applications : non-linearity , multi-axiality , hydration , temperature and drying effects,” *Cem. Concr. Res.*, vol. 79, pp. 301–315, 2016, doi: 10.1016/j.cemconres.2015.10.001.

[64] T. Vidal, A. Sellier, H. Cagnon, and X. Bourbon, “Experimental Investigation and Modelling Temperature Effects on Basic Creep of Concrete,” 2016.

[65] D. C. Drucker and W. Prager, “Soil mechanics and plastic analysis for limit design,” *Q. Appl. Math.*, vol. 10, no. 2, pp. 157–165, 1952.

[66] A. Sellier and B. Bary, “Coupled damage tensors and weakest link theory for the description of crack induced anisotropy in concrete,” *Eng. Fract. Mech.*, vol. 69, no. 17, pp. 1925–1939, 2002, Accessed: Jan. 28, 2012. [Online]. Available: http://www.sciencedirect.com/science/article/pii/S0013794402000693.

[67] A. Sellier, “Model FLUENDO3D Version 23-C for CASTEM 2017 Anisotropic Damage and Visco-Elasto-Plasticity Applied to Reinforced Multiphasic Materials, Technical Report,” 2018.

[68] D. Vo *et al.*, “Modelling the behavior of ASR affected structures using homogenized reinforced concrete finite elements,” in *16th international conference on alkali aggregate reaction in concrete, lisboa, 16-18 june 2020*, 2020, pp. 1–10.

[69] D. Vo *et al.*, “Evaluation of structures affected by Alkali-Silica reaction (ASR) using homogenized modelling of reinforced concrete,” *Eng. Struct.*, vol. 246, p. 112845, Nov. 2021, doi: 10.1016/J.ENGSTRUCT.2021.112845.

[70] A. Sellier, T. Vidal, L. Lacarriere, and H. Cagnon, “Modelling of prestressed concrete behaviour in the range 20-40°C,” in *Framcos’10*, 2019, pp. 1–10, doi: 10.21012/FC10.235516.

[71] A. Sellier and A. Millard, “A homogenized formulation to account for sliding of non-meshed reinforcements during the cracking of brittle matrix composites: Application to reinforced concrete,” *Eng. Fract. Mech.*, vol. 213, pp. 182–196, May 2019, doi: 10.1016/j.engfracmech.2019.04.008.

[72] V. Saouma, *Diagnosis & Prognosis of AAR Affected Structures*, RILEM Tech., no. to be published. RILEM, 2020.

[73] E. Grimal, A. Sellier, Y. Le Pape, and E. Bourdarot, “Creep, Shrinkage, and Anisotropic Damage in Alkali-Aggregate Reaction Swelling Mechanism-Part I: A Constitutive Model,” *ACI Mater. Journal-American Concr. Inst.*, vol. 105, no. 3, pp. 227–235, 2008, doi: 10.14359/19818.

[74] E. Grimal, “Cractérisation des effets du gonflement provoqué par la réaction alcali-silice sur le comportement mécanique d’une structure en béton,” Université de Toulouse, 2007.

[75] P. Morenon, E. Grimal, P. Kolmayer, A. Sellier, and S. Multon, “Modelling, assessement and rehabilitation of a a dam affected by an internal swelling reaction (ISR),” in *Third international Dam Wolrd conference, september 17-21, 2018*, 2018, pp. 1–10.

[76] P. Morenon, “Modélisation des réactions de gonflement interne des bétons avec prise en compte des couplages poro-mécaniques et chimiques,” Université de Toulouse, INSA, UPS, 2017.